Chhavi and Walker
Journal of Electric Propulsion (2024) 3:11
https://doi.org/10.1007/s44205-024-00073-2

Journal of Electric Propulsion

REVIEW **Open Access**

Review of non-conventional Hall effect thrusters

Chhavi Chhavi[1*] and Mitchell L. R. Walker[1]

*Correspondence:
chhavi@gatech.edu

[1] School of Aerospace Engineering, Georgia Institute of Technology, Atlanta, GA 30332, USA

Abstract

Electric propulsion has become the favored approach for Low Earth Orbit (LEO) maneuvers, resulting in substantial expansion in its use in the satellite industry. The Hall effect thruster's (HETs) high specific impulse and thrust-to-power ratio allow for a wide range of in-space propulsion applications, making it a viable alternative for various space missions. In the space sector, the mass production of HET is currently underway to fulfil the needs of the satellite industry for performing various maneuvers such as orbit boosting, station keeping, deorbitation, collision avoidance, and inter-orbital transfers. The increase in mass production has caused engineering challenges in manufacturing, necessitating an efficient batch production process to guarantee flight qualification within acceptable limits. Engineering production problems may cause manufacturing defects in HET components, leading to non-uniform magnetic field. The non- uniformities in the magnetic field can be observed azimuthally in the channel in various conditions resulting from electrical shorting and geometrical constraints. It is essential to comprehend the effect of such non-uniformities in the magnetic field on the performance of Hall-effect thrusters. An approach to understanding the potential effect of non-uniform magnetic field in HET is by analyzing the efficacy of non-conventional HETs possessing non-uniform magnetic fields. The article comprehensively reviews several non-conventional HETs with distinct channel cross-section geometries, such as linear, racetrack, and wall-less configurations. The paper presents a comparative analysis between non-conventional HETs and conventional HETs operating in low to mid-power configurations for performance evaluation. The review provides discussion of the effects of non-uniform magnetic field on the reduction of optimized HET operation by the presence of heightened erosion and reduction in stability. The review study highlights the importance of optimizing magnetic field topology for developing future thruster designs with enhanced performance and utilization.

Keywords: Hall Effect Thrusters, Magnetic Field, Non-Convention, Channel shapes, Linear, Racetrack

Introduction

The exploration of deep space has been a subject of enduring fascination; however, the pursuit of this endeavor has been impeded by technological constraints, causing it to be a formidable challenge to accomplish. Consistent progress in the aerospace sector and the creation of numerous satellites that necessitate efficient, reliable electric propulsion

(EP) demonstrate that EP is the most effective method for deep space expeditions as well as for commercial usage [1, 2]. Ongoing research and development of large thrusters, including the X3 [3] and HT20k [4] focuses on exploring novel concepts, designs, and providing this gateway for deep space missions. EP technology utilizes an electrical power source to generate electric and magnetic fields that accelerate the propellant to high velocities, resulting in high specific impulses, I_{sp}. The selection of the EP device for a mission is contingent upon the mission's specifications, which encompass a range of options, including thermal-electric thrusters such as resistojets or arcjets, as well as electrostatic and electromagnetic plasma thrusters like the Hall effect thrusters (HET) and gridded ion thrusters. The high specific impulse, thrust-to-power ratio, uncomplicated annular structure, and high efficiency of HETs have led to their widespread adoption in commercial space applications. The increased interest in HETs for use in commercial exploration prompted us to concentrate on HETs in this article [1, 2].

The 1960s was categorized as the beginning of the HET era. Morozov's work laid the groundwork for the development of fully functional HETs in the Soviet Union [5]. 1971 marked the subsequent successful deployment of HETs into space. Post-Soviet Russia witnessed a surge in the development of HETs, with thrusts ranging from 40 to 500 mN in 1982. The significant enhancement of their performance in 1991 resulted in an increased interest in HETs in many regions throughout the globe, including the United States, France, Italy, and Japan. This increased interest further led to extensive research in the operational ranges for HET varying from low power thrust levels, ~ 60 mN, to high power thrust levels, ~ 5.4 N. As the scope of space missions expands, the enhanced performance of propulsion systems with improved lifetimes has become the need of the hour. The future of HETs with even longer operating lifetimes will include high-power HETs for interplanetary missions and deep space exploration. However, the more extended life requirement leads to increased erosion of the channel walls by the high-energy ions, thus providing a considerable challenge.

EP has become the preferred method of propulsion for space exploration, leading to significant growth in the satellite business. According to references [6–8], the number of satellites orbiting in space has had a significant growth of 2300% between 2011 and 2020. As of January 2024, the satellite tracking website "Orbiting Now" has reported 8,377 operational spacecraft functioning in space. There is a growing demand for satellites to fulfil many roles, broadly classified as earth observation, space observation, and communication. In recent years, there has been significant growth in the small satellite constellation sector, with over 90 companies actively involved in promoting satellite constellations [9]. The proliferation of satellite constellations has necessitated significant bulk production. Figure 1 illustrates a substantial rise in the utilization of HET by satellites, with the number of satellite launches per year increasing from less than 5 in 1964 to 400 in 2020 [10]. These propulsion mechanisms are utilized for various maneuvers, including orbit boosting, station keeping, deorbitation, collision avoidance, and inter-orbital transfers. In the space sector, the mass production of HET is currently underway to fulfill the needs of the satellite industry. The rise in mass production has led to engineering difficulties in manufacturing, thus requiring a highly reliable batch production procedure to ensure flight qualification within acceptable tolerances. Engineering production issues can lead to manufacturing faults

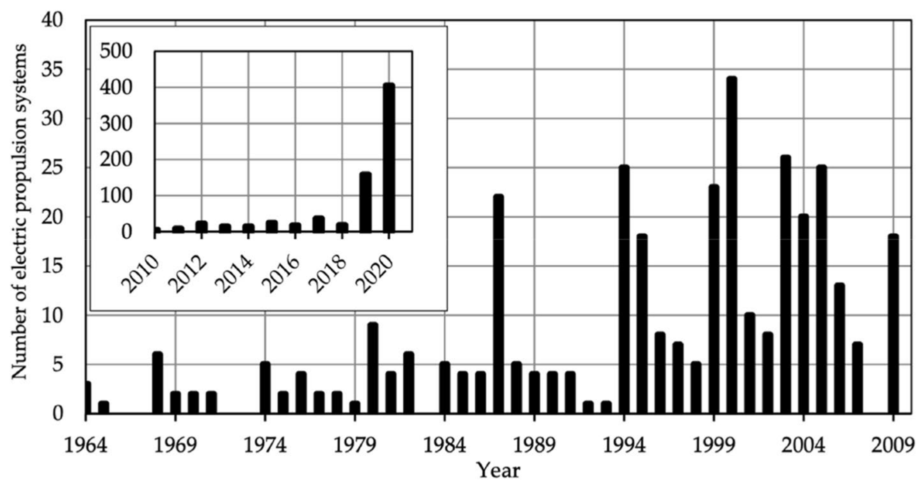

Fig. 1 Electric propulsion systems launched in space between 1964 and 2020 [10]

in HET components, resulting in a non-uniform magnetic field. The non-uniformities in the magnetic field can be observed azimuthally in the channel in various conditions resulting from electrical shorting, material processing, and geometrical constraints. Hence, an understanding of how a non-uniform magnetic field impacts the performance of HETs is necessary. Understanding the potential impact requires observation, and one way to do so is by analyzing the efficacy of non-conventional HETs possessing non-uniform magnetic fields based upon construction. Hence, there is a need to observe and study non-conventional HETs to evaluate the variations in performance of the thrusters in comparison to conventional HETs.

In order to address the intricate challenges at hand related to non-conventional designs, researchers devised several HET designs, including the X2 [11], X3 [3], Multi-channel HET [12], NASA-173GT [13], P5-2 [14], and others. While the essential operating concept remains the same, the configuration of HETs differs in terms of thruster size, number of channels [12], multi-stage operation (single, two stage) [13, 14], channel geometry such as linear, racetrack and cylindrical, ionization stage (DC and RF) [14, 15], Hall current closure mechanism such as open and closed, and magnetic circuits (coils and permanent magnets). Multi-channel thrusters, such as the X3 [3], give enhanced power density via concentric channels that can be operated concurrently. Nevertheless, the implementation of these channel configurations leads to notable operational complexities, including diminished packing efficiency, intricate channel interactions, and more. Scientists investigated two-stage HET design concepts to provide less complex solutions with the ability to fulfill mission requirements by increasing the overall thruster efficiency. NASA-173GT [13] and P5-2 [14] were designed as two-stage thrusters to optimize the ionization and acceleration processes found in HETs. However, a smooth transition between ionization and acceleration is highly challenging. The performance investigation of the two-stage thruster revealed excessive carbon contamination as a result of incorrect heat treatment of magnetic circuit material. Inadequate thermal management has a detrimental impact on the efficiency and stability of the thruster during long periods of operation. Diverse design solutions are currently under investigation to provide operational capabilities that will further increase the utilization of HETs.

This review article focuses on different discharge channel shapes for non-conventional HETs to understand the benefits and limitations associated with these shapes. The manuscript compares conventional and non-conventional HETs for the user to establish background knowledge regarding performance variation across different thruster designs focusing mainly on the effect of magnetic field. Differences in the design of HETs result in differences in the plasma physics associated with HETs. Section II presents a fundamental understanding of HET operation with a concise overview of the conventional HET and its operation mechanism. Section III delves into non-traditional designs, beginning with linear HET designs for Linear HET (LHET) [16], Linear Diamond HET [17], Linear Gridless Ion Thruster (LGIT) [18], and Planar HET (PHT) [19]. In contrast to the conventional HET, the linear design details specifics on open drift thruster operation with a notable variance in electron flow and magnetic field topology. In Section III, we also examine the converging and diverging HET designs CHT [20] and DCHT [21], provided with enhanced ionization and acceleration capabilities. The subsequent focus of our study pertains to the racetrack HET, explicitly examining its transition from an open electron drift mechanism to a modified closed electron drift mechanism. Busek BHT-RT-1500's racetrack HET [22] provides valuable insights into the wall erosion near the circular extremities and the non-uniform plume behavior observed during thruster operation. In order to mitigate the wall erosion present in the preceding racetrack thruster case, wall-less thrusters [23, 24] and narrow channel HETs [25] are examined in order to determine the potential benefits of channel-less thruster operation. To further grasp the potential of non-conventional designs, Section IV compares standard and non-conventional HET in terms of HET performance parameters. Section V of this study investigates the potential issues, such as stability and wall erosion, that may arise from employing non-conventional thruster designs. In Section VI, the future research direction for the non-conventional HETs is discussed.

The aim is to gain a better understanding of the impact of non-uniform magnetic fields on the performance of unconventional HETs and apply this knowledge to conventional HETs affected by manufacturing imperfections, aiding in performance prediction during satellite mass production. This review further highlights the significance of magnetic field topology optimization for conceptualizing future thruster design.

Conventional HET

Here we present the reader with the fundamental operating principles of the HET. These concepts serve as the baseline configurations for the discussion of the non-conventional designs. HETs are electrostatic devices that generate propulsion through the acceleration of ionized particles using an electric field. As illustrated in Fig. 2, the HET comprises four physical components, the anode, cathode, magnetic circuit, and ceramic discharge channel. The anode provides propellant to the discharge channel via apertured slots on the surface. The anode is also maintained at a positive potential utilizing an external power supply as demonstrated in Fig. 3. The cathode is an essential component of the system to supply the electrons to the HET. The cathode is maintained at a negative potential and located either externally or centrally, as depicted

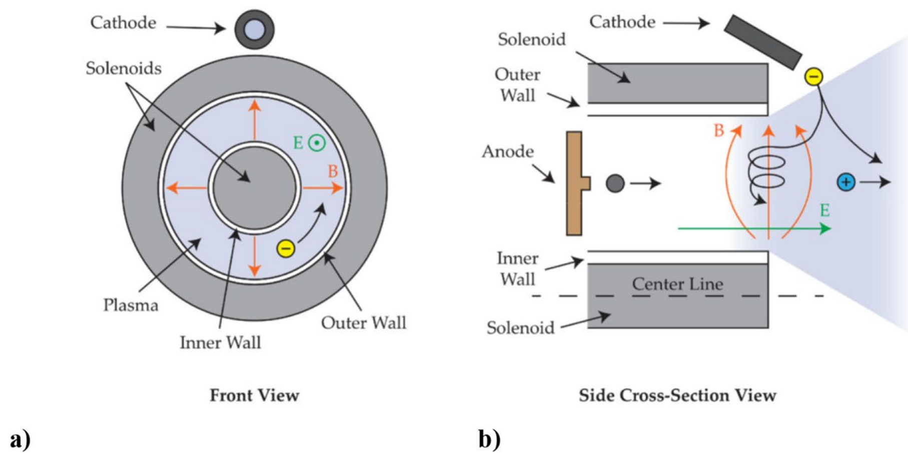

Fig. 2 The **a** Front and **b** Cross-sectional view of the conventional HET, as documented in Ref. [29]

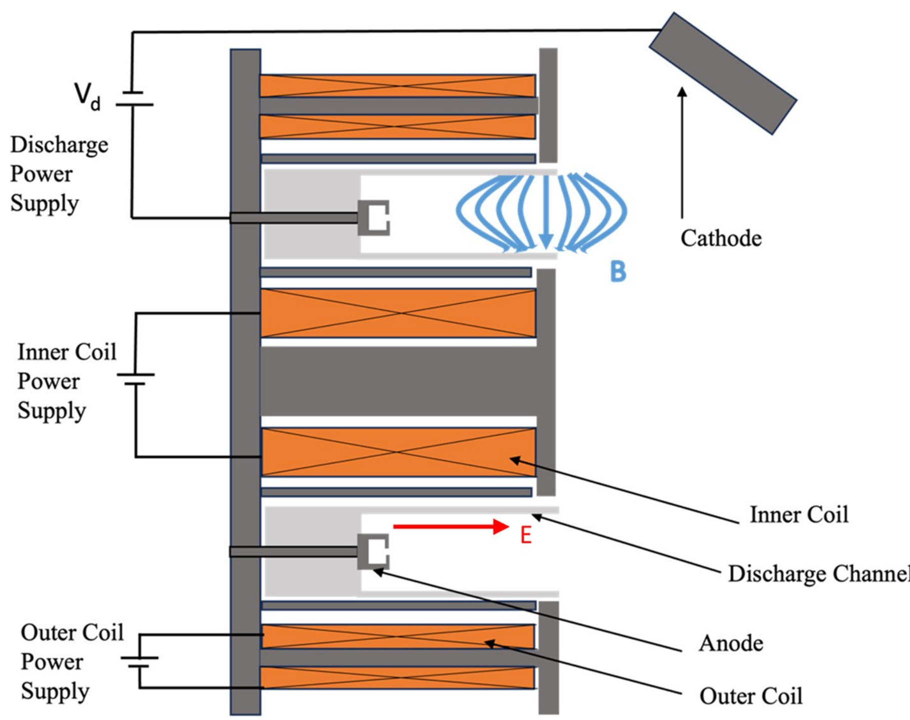

Fig. 3 Hall Thruster Schematic

in Fig. 4. It provides the electrons required for the ionization of the propellant gas and the maintenance of the plume's quasi-neutrality. The discharge channel of the HET, being ceramic, is primarily attributed to its electrical insulating properties, high thermal conductivity, and resilience to thermal shock. The discharge channel, being ceramic, has high secondary electron emissions when charged particles collide with the channel walls. The emission of these secondary electrons decreases the average electron temperature in the channel, thereby resulting in higher ionization efficiency as compared to thrusters with anode layer (TAL) through the extension of the

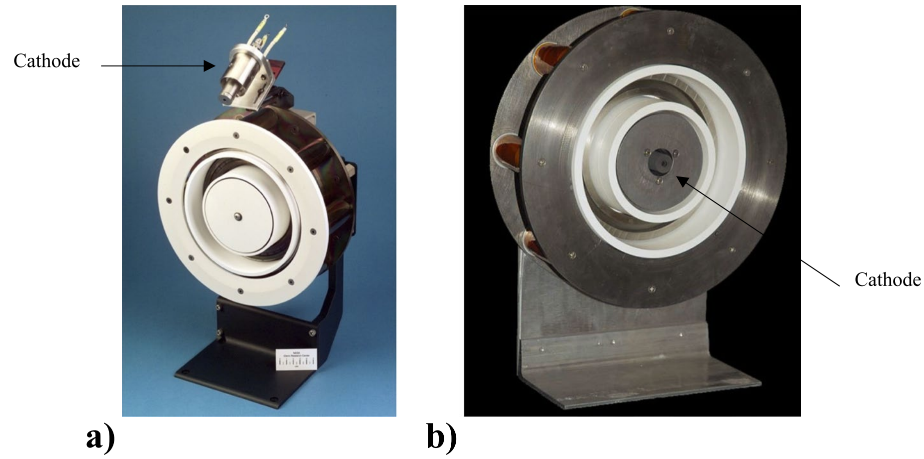

Fig. 4 The **a** NASA-173 M with externally mounted cathode [30] and **b** H6 with centrally-mounted cathode [31]

acceleration region affecting the potential distribution in the channel [26–28]. Lastly, the HET's magnetic circuit comprises inner and outer coils or permanent magnets. The magnetic circuit supplies the magnetic field required for electron confinement under steady operating circumstances.

The HET is named after the Hall current, that develops due to the well-known $E \times B$ drift of the guiding center when an electric field perpendicular to an applied magnetic field is present [32]. The generation of the electric field is achieved through the utilization of an external power source to sustain the potential difference existing between the cathode and the anode. The magnetically-confined electrons experience azimuthal drift due to the combined effects of the radial magnetic field produced by the magnetic circuit and the axial electric field. The collision between electrons and gas atoms leads to the ionization of the gas, which subsequently generates opposing currents of electrons and ions. The ions are accelerated by the potential difference caused by the electric field, resulting in thrust, and are neutralized in the plume by the electrons emitted from the cathode.

The HET operation consists primarily of the following three processes: 1) ion acceleration, 2) neutral particle ionization, and 3) plasma plume neutralization. The overview of processes mentioned above enhances the reader's comprehension of the mechanisms involved in plasma plume generation.

Ionization

The cathode supplies electrons through thermionic emission, and as the electrons leave the cathode, they possess distributions of thermal kinetic energy. The electric field generated within the discharge channel and the collisions with the propellant atoms influence the transport of electrons toward the anode. The electric field observed by electrons generated by the potential difference between the cathode and anode is called the discharge voltage. The presence of a magnetic field restricts the movement of electrons within the channel, leading to a closely confined drift motion of the electrons. In response to the $E \times B$ field, the guiding center of the electron experiences an azimuthal drift in the $E \times B$

direction due to the Lorenz force developed because of the electric and magnetic fields. The movement of electrons towards the anode increases the energy dispersion exhibited by the electrons—interaction with neutral atoms during electron travel results in inelastic collisions. The ionization of the neutral atom of the propellant occurs due to the interactions of electrons with energy equal to or greater than the ionization potential of the neutral atoms. Each ionization collision generates a low-energy electron and an ion. Following collisions, the electrons drift towards the anode, completing the circuit upon reaching the anode. Numerous variables influence ionization, including propellant type, electric field, magnetic field, and electron number density distribution. Ionization takes place in the vicinity of the maximal magnetic field region. The operational performance of the HET can be influenced by changes in the magnetic field, leading to alterations in the location of the ionization region.

Acceleration

Following the ionization process, the electrons undergo transverse movement towards the anode, while the ions experience acceleration towards the exhaust due to the establishment of an electric field within the system. The electron density distribution varies axially in the axial direction and peaks at the thruster exit plane where the local magnetic field intensity is greatest. The observed potential difference in a localized region is due to variations in electron number density distribution. Consequently, this leads to the acceleration of the ions towards the thruster's exit plane. The mobility of the ions remains unaffected by the magnetic field because of their greater Larmor radius compared to the thruster dimensions, which is a consequence of their substantial mass. The equation for the Larmor radius is as follows:

$$r_L = \frac{mv_\perp}{B|q|} \tag{1}$$

The acceleration of the ions depends on the amount of discharge voltage utilized by the ions for acceleration. Therefore, the acceleration voltage, which typically ranges from 60 to 85% of the discharge voltage, V_d, significantly impacts the impulse, thrust, and voltage utilization efficiency of the thruster. The processes of acceleration and ionization are intricately linked and lack distinct limits in the context of standard HET operation.

Neutralization

The ions expelled from the thruster at high speeds create a positively charged cloud. Neutralization is required to prevent charge accumulation on the spacecraft and thruster and to preserve the quasi-neutrality of the plasma plume. The cathode supplies electrons to the plume to achieve quasi-neutrality. The electrons recombine with the ions resulting in the neutralization of the ion beam and production of quasi-neutral plasma plume, which ensures a charge-neutral operating environment.

Non-conventional HETs

The need to develop a propulsion system with high efficiency for small satellites has resulted in the development of low-power HET technology. While the core operating concept remains the same, alternative designs of the HET channel aim to provide improved packing efficiency as well as advantages that improve HET operation.

Numerous design initiatives have led to the investigation of various methods for enhancing HET operational capabilities. To increase the thruster's overall efficiency, the two-stage HET is developed as the result of investigation of the separation and optimization of ionization and acceleration independently [14]. The spacecraft employs many hall thrusters during operation. The circular shape of the HET channel leads to low packing efficiency, resulting in wasted space. Proposed modifications to the discharge channel shape aim to optimize the packing efficacy of HETs. Numerous research projects have investigated the performance of different channel shaped HETs. In this study, the authors want to highlight these non-conventional channel-shaped HETs and review the following channel shapes: linear, cylindrical, racetrack, and wall-less.

Linear channel HETs

A rectangular slit is the discharge channel in the linear HET architecture, with electrons traveling from an emitter to a collector side. Open drift is the electron motion pathway in such HETs that necessitates a strong magnetic field for effective ionization and acceleration. The linear HETs with open drift design exhibit a deviation from the typical Hall parameter values of 10–100 and instead operate with a Hall parameter of unity. In the case of linear HETs, the primary function of the cathode is to neutralize the ion beam rather than to provide electrons for ionization due to the presence of additional emitter electrodes [16, 19]. The compact design of the linear HET aims to enhance stacking efficiency and expand the propulsion system's operating environment. The compact nature of the linear thruster geometry offers further advantages, including simplified construction and easier magnetic field optimization. The subsequent discussion on linear thruster designs offers valuable insights into the operational characteristics of HETs featuring a planar discharge channel. The thrusters reviewed in this section are LHET [16], LHET diamond -walled [17], LGIT [18] and PHT [19].

The Linear Hall Effect Thruster (LHET)

With the growing demand for low-power thrusters on small satellites, Hargus and Cappelli [16] provided an in-depth analysis of fundamental scaling physics and its effect on the discharge operation of the thruster, that is crucial. The application of the scaling methodology was employed on a linear thruster that was constructed based on the design concepts of an existing co-axial HET as shown in Fig. 5. The LHET was successfully operated by Hargus [16].

The linear HET design was based on a scaling factor of 0.1 in relation to a co-axial thruster with a nominal power range of 500–700 W. The thruster is comprised of four 90-mm long electromagnet copper windings with 9.5-mm diameter cores of commercially pure iron and top and bottom magnetic pole plates made of 3-mm thick stainless steel. The magnetic circuit is interconnected to provide a horizontal magnetic field over the alumina acceleration channel [16]. The insulator, measuring 4 mm in

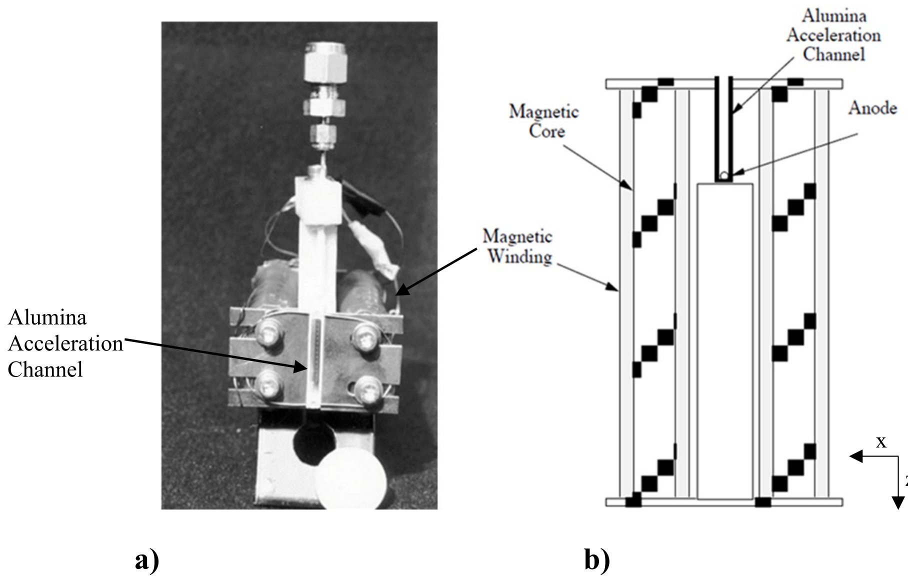

Fig. 5 **a** Photograph of LHET **b** Cut away view of LHET design [16]

width and 22 mm in depth, is supported by a phenolic block. The lower and terminal surfaces of the channel are affixed to alumina plates measuring 0.5 mm in thickness, thereby constituting the lateral boundaries. The anode utilized in the experiment consists of a stainless-steel tube with a diameter of 1.6 mm. It has 14 propellant feed holes, each with a diameter of 0.2 mm. These feed holes are evenly placed with a center-to-center distance of 1.6 mm. An Ion Tech, Inc. HCN-252 hollow cathode is employed as the ion beam neutralizer. The cathode is installed on a stainless-steel bracket in front of the thruster, with the hollow cathode exit 1 cm above the acceleration channel exit. The mass flow rate of xenon during the neutralization process is 0.4 mg/s.

In order to comprehend the functioning of the linear HET, it is assumed that either the average electron energy or the electron temperature remains constant. The experiment uses a current control method, employing tantalum wire to achieve the required closure in the Hall current. The tantalum wire looped around the discharge channel serves to short the electron current between two side walls of the channel near its end plane.

Due to the unsuccessful operation of the thruster, caused by the design constraints under which it was developed, an oscillating mode with a period of 0.1 to 1 s was generated at an operating power of 500 to 700 W. A 1300 μF capacitor is incorporated into the anode power line to function as a low-pass filter, separating the plasma from the anode power supply. The capacitor enabled the thruster to function with some stability at 250 V. The brief period of stable functioning yielded a thrust of 2.2 mN and a specific impulse of 1040 s when subjected to a magnetic field intensity of 1600 G. However, the operational parameters deviated significantly from the design conditions established for operation of the thruster, leading to an overall efficiency of 14.6%, considerably lower than the anticipated value. After operating in such a

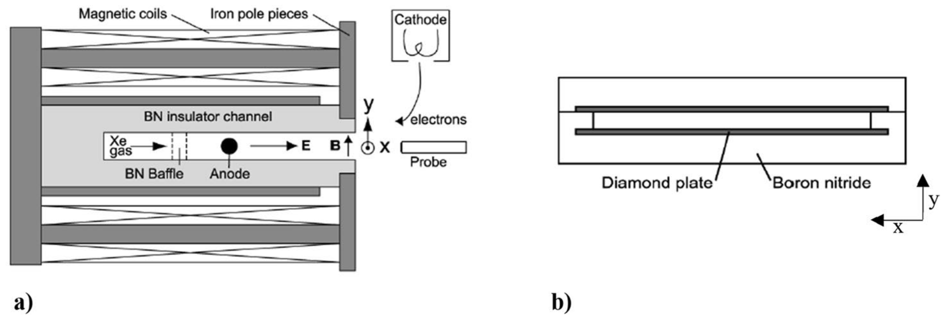

Fig. 6 **a** Design details of linear HET with BN channel and **b** Schematic configuration of diamond channel [17]

condition, difficulty in restarting the thruster was encountered, leading to the discharge being extinguished.

The pulsing activity was interpreted as a basic wall charging event, which was limited by the classical conduction of electrons to the side wall. As a result of charge building, a capacitive sheath created at the wall was believed to be the cause of the pulsing behavior. The phenomenon of charge accumulation was seen on the walls of the discharge channel. However, the effect of capacitive sheath development still needs to be investigated. According to the explanation given, the inability to close the Hall current is stated to be the potential cause for the inability to have continuous and stable operation. The LHET offers valuable perspectives on the developmental procedures related to a linear channel design for HETs. However, significant efforts are required to establish a LHET that functions reliably and is capable of flight qualification.

Linear HET with diamond discharge channel

The downsizing of the HETs for low-power operation, as employed in LHET [16], presents several challenges. These include increases in particle and energy flux towards the ceramic walls that result in erosion and a reduction thruster lifetime. Meezan [17] proposed a solution for reducing erosion in small-scale co-axial thrusters. A linear open drift design was proposed with advanced ceramic materials such as polycrystalline diamond. In order to reduce the channel erosion rate, the revised design aimed to comprehend the ion beam current and propellant utilization for different wall materials. The substitution of the conventional boron nitride (BN) ceramic channel with diamond, which possesses a low dielectric constant and a low backscatter coefficient, was proposed to offer the favorable characteristics required for HET walls. The sputter resistance of diamond under ion bombardment at the exit of the HET is approximately 25% more than that of BN. Two distinct discharge channels were fabricated to facilitate the examination of various wall materials. The initial channel comprised a rectangular BN enclosure of roughly 50.8 mm in width, 3.2 mm in height, and 12.7 mm in length as shown in Fig. 6. The second channel is fabricated to include two pockets designed to accommodate rectangular plates composing of various wall materials, such as the diamond wall layer. These plates could be securely fastened within the channel.

The diamond thruster utilized slabs of pure chemical vapor deposition (CVD) diamond with a thickness of 1 mm. The magnetic circuit comprised a pair of rectangular solenoid coils, two front pole pieces, one back pole piece, and a magnetic screen. A commercial Veeco/IonTech HCN-252 hollow cathode discharge neutralizer was used to neutralize the ion beam with a mass flow rate of 0.3 mg/s of xenon [17]. The cathode, positioned at the center of the x-axis, was 45 mm away from the channel in the y-direction and 28 mm downstream from the channel exit.

The operation of the two distinct thrusters with identical operating voltage, 250 V, and mass flow rate of xenon, 0.6 mg/s, resulted in the diamond-walled thruster having discharge current of 0.34 A providing propellant consumption of only 78%, about 25% lower than the classic thruster. The ion current-to-discharge current ratio of the diamond thruster is 0.33, remarkably similar to that of the conventional thruster, 0.38, thus validating the 14.6% thrust efficiency prediction. Despite the limited data, the erosion rate of diamond is 0.002 mm^3/°C lower than that of BN at incident ion energies of approximately 400 eV. Plume divergence angles of 15 degrees in the transverse, parallel to the magnetic field, direction and 60 degrees in the lateral, parallel to the $E \times B$, direction were measured. The difference in lateral and transverse divergence angles was believed to be a geometric trait of these linear geometries. Breathing oscillations with a frequency of 35 kHz were recorded in the BN thruster when operated at a discharge voltage of 250 V. The diamond-walled thruster, on the other hand, was unable to operate below a discharge voltage of 200 V because the discharge current oscillations became extremely unstable to the point of plasma extinction. As a result of the inability of the diamond thruster to function below 200 V and the diminishing magnitude of the oscillations as the voltage increased, the oscillations were not discernible in the case of diamond LHET. Resulting in stable operation of diamond LHET above 200 V.

The experiments revealed notable distinctions in the current–voltage (I-V) characteristics between the diamond channel thruster and the conventional HET. The diamond thruster exhibited a reduced discharge current of 0.3 A at 300 V compared to its BN counterpart with discharge current of 0.45 A. The linear design of the HET led to a significant lateral divergence, resulting in an asymmetric beam. This characteristic may cause issues for adjacent satellite components and present difficulty in integrating the thruster into a mission. Hence, the influence of beam divergence in the context of linear geometry can be regarded as a prominent factor contributing to the operational inefficiencies of linear HET systems. The promising results exhibited by the diamond thruster offer a means to investigate alternative wall materials for non-conventional thruster configurations.

Linear Gridless Ion Thruster (LGIT)

The demand to enhance throttle capability and efficiency prompted the conception of two-stage HET design concepts. Beal [18] designed a Linear Gridless Ion Thruster (LGIT) that integrated the ionization stage of a gridded ion thruster with the acceleration stage mechanism of HETs as shown in Fig. 7. The LGIT's goal was to increase the HET's overall efficiency and throttle ability through proper decoupling and independent optimization of the two stages. By employing a dual-stage configuration, the usage of an electric field for ion acceleration enables higher thrust density, hence enhancing the throttability offered by LGIT. The distinctive linear discharge chamber facilitated the magnetic circuit's development. By incorporating an intermediate electrode in the discharge channel, the two-stage design is included in the linear geometry to achieve greater control over the ionization process. The role of the intermediate electrode is to facilitate ionization and acceleration by acting as a cathode and an anode, respectively.

The ionization stage is composed of a standard NASA 6.4-mm diameter hollow cathode, centrally positioned within a rectangular chamber serving as the anode. On the other hand, the acceleration stage resembled the traditional HET. The distinct magnetic field topologies are implemented in each of the two stages of the thruster. The first stage of the thruster, the ionization stage, employs cusped samarium-cobalt permanent magnets. An increase in the effective path length between the cathode and anode walls of the ionization stage leads to enhanced ionization. The HETs acceleration stage uses a transverse magnetic field to obstruct electron transport toward the anode. The configuration of magnets ensures a symmetrical exhibition of the magnetic fields throughout the midplanes of the thruster. Five magnets are placed about and below the anode, while one magnet is placed on each side of the anode for a total of twelve magnets.

Although the thruster is designed with two stages to operate within a 2-kW range, the experiments used a single-stage configuration because the team was unable to acquire a hollow cathode for the ionization stage of the thruster prior to the experimental performance characterization Consequently, the thruster was utilized in a single-stage configuration, resembling a conventional HET. The thruster was operated at a discharge voltage of 300 V while the electromagnets were functioning at 50% of their nominal design current. The anode and accelerator-cathode volumetric flow rates were set to 15 and 6 sccm of xenon, respectively. With the cathode floating at 25.5 V below ground, the thruster detonated in this configuration produced a discharge current of 3.9 A at a discharge power of 1,170 W. The thruster maintained a stable discharge plasma for roughly three minutes.

An electrical short between the anode and the screen of the magnetic circuit extinguished the discharge and prevented further optimization of the performance through optimization of the magnetic field. The experimental results included a measured thrust of approximately 20 mN, a specific impulse of around 1,400 s, and an anode efficiency of 12% during the three minutes of stable discharge. The observed lower anode efficiency as compared to the conventional HET can be attributed to the

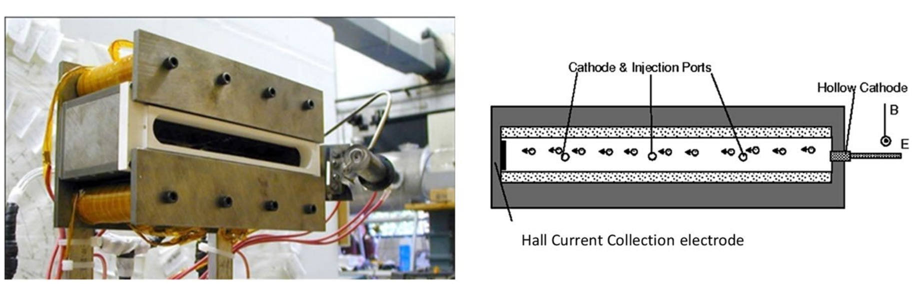

a) b)

Fig. 7 **a** Photograph of LGIT and **b** Front-view of linear acceleration stage of LGIT [18] utilization of a single-stage operation rather than the initially envisaged two-stage mode of operation. The true performance capabilities of the concept remained unrealized due to the unstable operation of the LGIT. Modifications are required to ensure consistent and reliable performance of the thruster.

Planar HET (PHT)

Rovey [19] conducted research to comprehend the electron dynamics in E × B devices in order to facilitate the elimination of annular channel complexities; this research led to the creation of a planar HET (PHT) with a rectilinear configuration Fig. 8. The design was speculated to successfully mitigate electron transport losses that were reported in annular thrusters as a result of their curvature.

The PHT is a planar device that injects Hall current electrons into the thruster channel via ports on the sidewalls and a collector electrode on the opposite side to form a closed circuit. The emission of electrons occurs via a diminutive aperture with a diameter of around 3.2 mm. Electron extraction is facilitated by using titanium collector plates recessed into the collector side wall, located on the opposing side of the thruster. A neutralizing device is positioned on the collector side of the thruster at roughly 5 cm from the thruster and 10 cm from the exit plane. The shape and magnetic circuit under investigation were initially constructed with xenon as the working gas and five sliding plates functioning as recessive joints. The circuit consists of two hollow emitter electrodes, a cathode, and three collector plates. The channel is fabricated using ceramic plates made up of baked alumina silicate, with dimensions of 203 mm in length, 25 mm in width, and 108 mm in depth.

Furthermore, there are four Langmuir probes alongside the emitters and collectors, with two probes positioned on each side wall. Elastic tongues affixed to the primary pole piece secure the walls in position on the emitter and collector sides. The functioning of the PHT exhibits similarities to that of the standard HET, with the exception of the mechanism employed for circuit closure. In the context of PHT, the introduction of thermionically excited electrons occurs by means of insertion from a single side of the channel. The electrons interact with the propellant gas and subsequently accumulate on the opposing side of the channel.

The performance of the thruster was characterized at discharge voltage, discharge current, and maximum radial magnetic field of 100 V, 5 A, and 100 G, respectively. As the volumetric flow rate of xenon at the anode increased from 12.5 sccm to 25 sccm, there was a corresponding decrease of 20 V in both the floating voltages of the

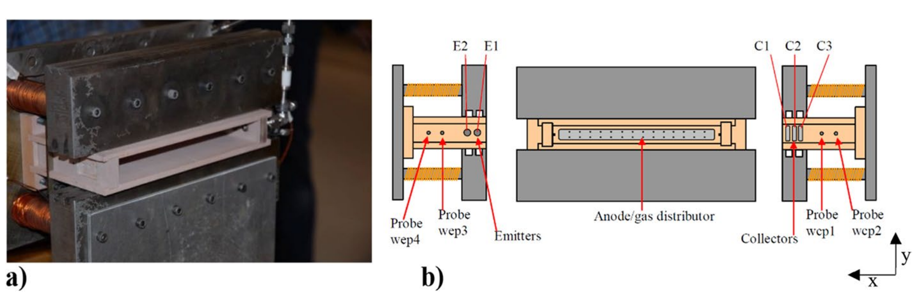

Fig. 8 **a** PHT and **b** Schematic of PHT with side views of emitter and collector placements [19]

emitter and the most-probable ion voltage. The PHT exhibits consistent performance across a broad range of discharge voltages, specifically between 50 and 150 V. While operating the thruster at the start-up module, it was observed that in the absence of a magnetic field, an increase in the anode current and voltage led to the visible plasma being shifted towards the exit plane of the thruster. Ion energies ranging from 50 to 65 eV were acquired during the operation of a 100 V discharge, with a peak in the flux distribution occurring at an off-axis angle of 15 to 20 degrees. Despite the absence of performance data, it was noted that the PHT exhibited a uniform ion current density profile, diverging from the typical double-peak depiction of ion current density distribution seen in traditional HETs. The observed ion current density profile is attributed to ion generation occurring at the emitting side and ion accumulation occurring at the collection side. As the magnetic field increases, the PHT exhibits a notable departure from the standard HET in that it fails to achieve a minimum discharge current. More experiments are required to evaluate the difference in the performance of the PHT and standard HET designs to infer the decrease in complexity in the case of varied discharge channel shapes.

Cylindrical channel HETs

The scaling of HETs for low-power operation has always posed challenges with respect to channel erosion and heating of thruster parts [33]. These issues are accentuated due to the unfavorable ratio between the surface area and volume of the channel. In order to optimize energy efficiency in low-power operation, Cylindrical Hall Effect Thrusters (CHT) were explored [20, 21]. CHTs were developed based on the conventional HET with closed drift mechanism allowing for Hall parameters closer to 10.

Cylindrical HET (CHT)

Raitses et al. [20], at the Princeton Plasma Physics Laboratory (PPPL), successfully created a cylindrical discharge channel with a uniform cross-section. The motivation for the CHT design was to lower the channel surface area-to-volume ratio in order to reduce ion losses by limiting electron motion [33, 34, 35]. Extensive research has been conducted on this unconventional design in multiple regions of the world, including Japan [36], Germany [37] and Korea [38].

The design of the cylindrical thruster is based on the closed $E \times B$ electron drift idea, with a Hall parameter of 16, which resembles the traditional annular HET. However, the operational characteristics of the electron drift closing mechanism are dissimilar. PPPL developed two variants of varying sizes for the CHT thruster. As illustrated in Fig. 9, these 9-cm and 2.6-cm thrusters are powered at 1 kW and 100 W, respectively.

The study [20] centers on a 2.6-cm thruster operating at extremely low power. The CHT comprises a cylindrical ceramic channel, a magnetic core, and a ring-shaped anode that acts as the gas distributor as shown in Fig. 10. A cusp magnetic field is generated within the channel using electromagnetic coils with the opposite current. The magnetic mirror obstructs the electrons from penetrating the annular section with the anode due to the field distribution that causes the electrons to bounce oscillate in the axial region. The length of the annular region is designed to minimize the ionization mean free path for localization of the ionization process. In order to sustain ionizing collisions, the anode is positioned within a small annular segment of the thruster.

To study the thruster operation for low power conditions, the thruster is operated at 17 sccm of xenon with a background pressure of 17×10^{-6} Torr. The thruster performance is characterized across a wide variety of operational settings, encompassing discharge voltages from 100 to 300 V and volumetric flow rates from 10 to 30 sccm. The discharge voltage, mass flow rate, and magnetic field are varied in order to sustain a thermally stable state for an estimated duration of one hour. At a discharge voltage of 250 V and mass flow rate of 2 mg/s, the thruster achieves an efficiency of roughly 22% [39]. At low, 10^{-5} Torr, background pressure, the thruster increases in thrust for constant discharge voltage as the discharge current decreases. The observed variation was attributed to the alteration in the configuration of the magnetic field, transitioning from a cusp to a direct configuration [40]. The efficiency of the cylindrical thruster at the 100-W power level, anode efficiency 22%, is comparable to and in some cases greater than that of the conventional annular low power thruster, such as the BHT-200-X2B (anode efficiency 21%) [41], SPT-30 (anode efficiency 22%) [42], KM-37 (total efficiency 24%) [43], and KM-20 M (total efficiency 30%) [44, 45].

Notwithstanding its encouraging outcomes with respect to thruster efficiency, a significant limitation of the cylindrical design is the substantial beam divergence of 70–80 degrees of the plasma plume [39]. The cause of considerable beam divergence is attributed to a robust radial electric field that facilitates the escape of ions at significant angles of 70–80 degrees. Electrons are no longer compressed in the axial position in the case of CHT, which lead to problems like plasma instabilities. The cylindrical thruster operation exhibits a lack of significant oscillations at a frequency of 20 kHz. Additionally, the CHT exhibits a high propellant utilization rate of 67% [39] at the same mass flow rate as conventional annular HET, 47%, making it a potentially viable design for low-power operation. Nevertheless, expanding this design for high-power operations raises potential issues of high beam divergence as well as thruster ignition.

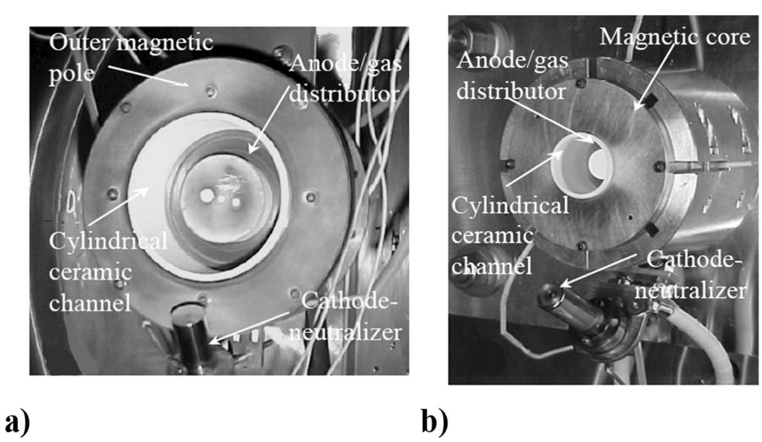

Fig. 9 **a** 1-kW CHT and **b** 100-W CHT [20]

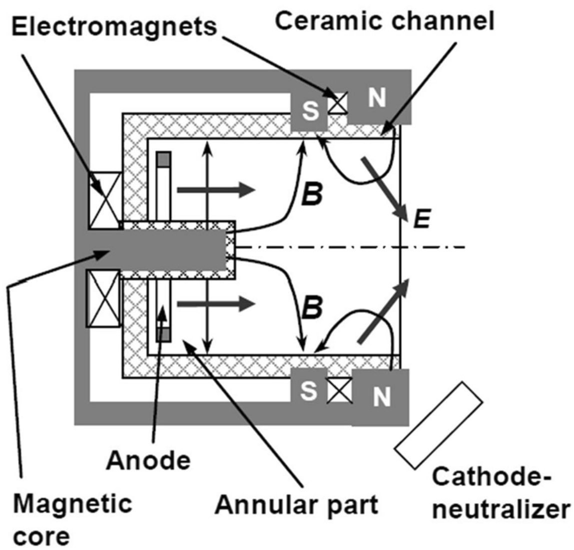

Fig. 10 Schematic of CHT components [20]

Diverging Cylindrical HET(DCHT)

Cusp field thrusters, such as the CHT [20] and High-Efficiency Multi-Stage Plasma (HEMP) thruster [46, 47], have yielded valuable findings regarding the advantages of the cusp field design, including ionization localization and enhanced propellant utilization. To conduct a more comprehensive assessment of the advantages associated with the cusp field arrangement, a novel non-conventional HET was designed, featuring a diverging channel as shown in Fig. 11. In particular, an experimental cusped field HET was built by Courtney [21] in order to investigate the impact of alternate magnetic circuit arrangements.

The optimization of the propellant feed, anode, and propellant system is divided into two independent system elements. The anode is positioned at a distance of 4 mm from the core stem, while the fuel propellant line is situated farther away from the core. The thruster consisted of three magnetic patterns grouped in a diverging manner, resulting in two separate magnetic field cusps with strong magnetic bottling around the anode. The researchers hypothesized that the implementation of a diverging design would contribute to the mitigation of wall ion losses by offering a larger surface area, as well as leveraging the advantages of the cusp field, as outlined in the CHT thruster study [20]. The diverging configuration of the channel leads to the generation of a gradient in the distribution of the magnetic field.

The thruster is operated at a volumetric flow rate of 8.5 sccm of xenon and a discharge voltage of 250 V for two hours. A Busek hollow cathode was employed to operate the thruster. The thruster was subjected to a broad range of power conditions, from 102 to 538 W. A transition point was identified at 450 V at 10 sccm, resulting in an anode current deviation as the anode potential is increased. As a result of decreasing the mass flow rate from 10 to 7 sccm, the transition point shifts from 450 to 410 V. The investigation identified arching between the thruster and cathode at a flow rate of 10 sccm and an anode voltage of 400 V. At a discharge voltage of 550 V, the thruster achieves a maximum efficiency of 44.5% at 13.4 mN of thrust. The performance of DCHT is similar to the Busek BHT-200 [48], a more typical HET that produces 12.8 mN of thrust at a total efficiency of 43.5% at 200 W. The DCHT exhibits similar performance to that of the THALES HEMP thruster, which achieves an anode efficiency of approximately 31%. The HEMP thruster generates a thrust of around 12 mN with a xenon volumetric flow rate of 10.0 sccm at 400 V [46].

While the performance of the DCHT thruster is similar to that of conventional HETs, there are few mentions of erosion concerns in the vicinity of the anode. Sputtering deposition is detected by the darkening of the channel near the anode. Although there is evidence of discoloration, the decrease in erosion over the length of the channel yielded positive outcomes in terms of concentrating plasma ions at the center and offers a viable approach for decreasing wall erosion.

Racetrack channel HETs

As the thruster operation transitions from low to high power, conventional annular HETs encounter unfavorable thrust density scaling issues. As a result, the necessity to develop a novel non-circular topology for thrusters has grown. One of the motivations for designing such thrusters is the need for a longer ion-neutral collision mean free path than the acceleration length for ions, necessitating lower plasma density.

BHT-RT-1500

To address such limitations, Pote [22] at Busek Co. Inc. initiated the development of a novel non-circular racetrack HET, BHT-RT-150, and later on, a higher aspect ratio design, BHT-RT-1500 as shown in Fig. 12. The racetrack geometry consists of semi-circular halves of the conventional circular HET connected by straight sides, giving a symmetric racetrack cross-section. This unique discharge geometry is believed to increase geometric flow area by scaling the thruster only in the linear direction so as to eliminate the negative thrust density scaling trends. The racetrack geometry fulfills the specified criteria, which includes a small ion gyroradius, a continuous closed electron drift

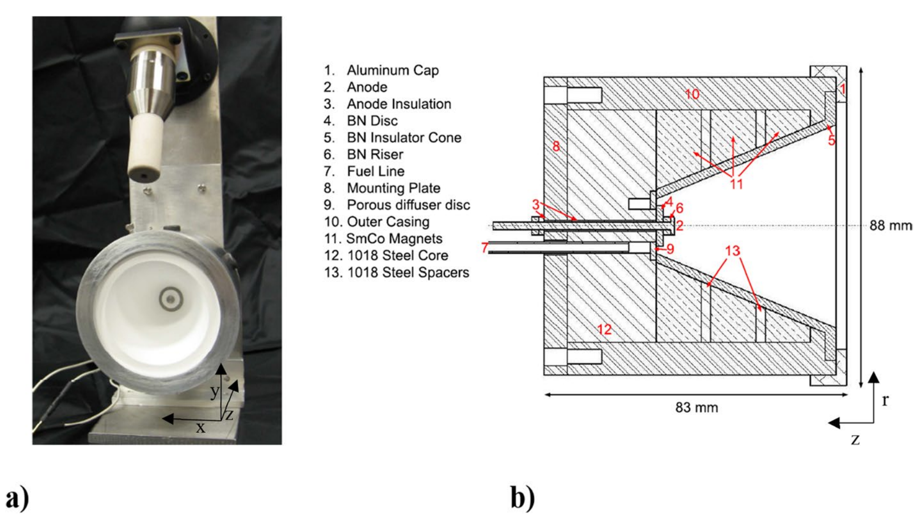

Fig. 11 **a** DCHT with Busek hollow cathode and **b** Cross-section view of DCHT components [21]

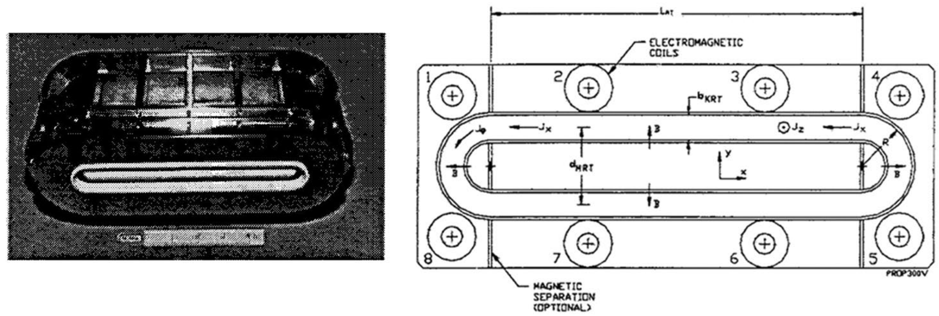

a) b)

Fig. 12 **a** BHT-RT-1500 and **b** Front view schematic of racetrack channel of BHT-RT-1500 [22]

plasma, and the prevention of electron collisions with the walls. These factors present compelling evidence for the potential of racetrack geometry to exhibit performance on par with that of the standard HET.

The racetrack HET exhibits comparable behavior to the conventional HET in terms of thrust-to-power ratio and I-V changes at low voltages. The thruster produces an 84 mN thrust at 1,675 W and 350 V discharge with a single magnet coil, equating to an anode efficiency of over 41% and an anode-specific impulse of 1,678 s. Unfortunately, non-uniform discharge characteristics are observed at elevated discharge voltages. The discharge intensity increases in the curved sections of the racetrack, accompanied by a noticeable abrupt change in the brightness of the plasma at the upper left and lower right corners. A uniform magnetic field magnitude and a uniform flow distribution at the centerline leads researchers to attribute the asymmetric brightness to the electron drift motion. An additional factor suggested to play a role in the observed non-uniformity is the radial fluctuation of the B-field. The radial magnetic field exhibited minimal gradient throughout the straight segment of the racetrack, while a substantial gradient is present in the curved segments. This observation implies the necessity of optimizing the magnetic field topology across the channel.

The BHT-RT-3000 Racetrack thruster was also tested in the Busek study. A commercial Ion Tech 1/4-in. hollow cathode is positioned above the core of the thruster during operation. The thruster is operated within a power range of 1500 W to 4000 W with a mass flow range of 5 to 12 mg/s of xenon. The power levels are achieved by maintaining a discharge voltage of 300 V. At the designated operational condition of 3000 W, the thruster generates a thrust of 180 mN, exhibiting a specific impulse of 1950s and an anode efficiency of 57%. At high mass flow rates, the discharge current and mass flow rate deviate from their expected linear behavior.

According to the discharge plume measurements, the electron number density of the central jet is greater than that of the surrounding jets. Non-uniform plasma discharge is observed across the channel, indicating that the magnetic field in the semi-circular end sections and the straight portion of the racetrack should be optimized for better performance. The racetrack thruster demonstrates the importance of B-field topology and highlighted the need for magnetic circuit tuning to improve non-circular thruster performance [49].

Wall-less channel HET

Wall erosion, a common issue observed in the thruster discussed so far, is tackled by the development of an alternate wall-less design that shifts the ionization and acceleration regions outside the plasma chamber. This section reviews WL-HET [23], XPT [24] and NCHT [25].

Wall-less HET (WL-HT)

Mazouffre [23] created a wall-less thruster by relocating the anode toward the channel outlet without affecting the magnetic field topology shown in Fig. 13. The design of the prototype is derived from a 200 W-class HET, which produces a thrust of 10 mN at a voltage of 200 V at a xenon mass flow rate of 1.0 mg/s. The thruster demonstrates four notable characteristics that contribute to its versatility. First, the magnetic field is generated via small samarium-cobalt magnets on either side of the channel walls—the manipulation of the number of magnets allows for convenient modification of the magnetic field strength.

Second, the homogeneous injection of the propellant gas is achieved via a porous ceramic material positioned at the back of the channel. Third, a central copper heat sink is employed to evacuate heat towards a radiator placed behind the thruster. Finally, the channel width may be adjusted using different sets of ceramic rings. The anode employs in the wall-less prototype consists of a stainless-steel ring with a width of 5 mm. The anode is wound along the outer perimeter of the channel exit plane, which corresponds to the location with the largest amplitude of the magnetic field. The cathode utilized in this study is a hollow cathode with a LaB_6 inlay. The cathode orifice is positioned at a radial distance of 10 cm below the thruster symmetry axis and an axial distance of 3 cm from the channel exit plane.

Under the operational parameters of 200 V discharge voltage and 1 mg/s xenon mass flow rate, plasma discharge occurs beyond the dielectric cavity of the thruster, and the ion beam boundaries became less distinct. The WL-HT's average discharge current is 0.16 A higher at 200 V and 0.24 A higher at 260 V than a standard thruster. Numerous magnetic field lines, particularly those stretching downstream, interacted with the anode, increasing the electron mobility towards the anode. Observations also reveal elevated radial ion current and ion species with higher charges. The ion beam energies obtained for the WL-HET and standard HET are 120 eV and 160 eV, respectively. Comparing the two HET configurations, poor energy conversion due to 40 eV lower ion beam energy is identified as a potential cause of beam divergence concerns in the region of severe curvature of magnetic field lines. Although the acceleration region is relocated downstream beyond the exit plane, there is still a significant particle flux towards the walls at the anode location. Therefore, it is proposed that optimization of magnetic field topology is necessary [50]. The absence of walls in the design exhibits notable advantages in terms of facilitating the expulsion of the discharge to the exterior. However, this divergence is substantial, resulting in a discharge current that exceed the nominal values by 0.84 A. Additionally, the heightened interaction between the plasma and the thruster poles poses significant limitations on the performance of the thruster.

External discharge plasma thruster (XPT)

As observed in prior studies, the wall-less geometry approach entails relocating the anode to the exit plane to mitigate the erosion of the HET walls. However, a significant degradation of the polar regions was yet observed. Karadag [24] advocated the utilization of an alternate electric thruster design known as the external discharge plasma thruster (XPT) as a potential solution to address this particular concern. The XPT propulsion system as shown in Fig. 14 was characterized by a non-anodic cavity, which generated and maintained a plasma discharge external to the thruster's physical structure. The ionization and acceleration phenomena occurred externally to the structure without a discharge route.

In contrast to prior wall-less configurations, the anode of the thruster in question was extended beyond the exit plane, with the highest intensity magnetic field positioned upstream of the anode. The thruster lacked a magnetic core, associated power supply, and a nonuniform propellant feed. The XPT was designed with a streamlined structure to address the challenges of erosion and scaling in HETs, offering innovative solutions that eliminate the need for walls.

The XPT designed with an annular geometry included a positive electrode that supplied propellant, a negative electrode, and permanent magnets. The prototype had an anode with four slots for propellant distribution, along with a front wall made of boron nitride measuring 2 mm in thickness. An IontechHCN-252 hollow cathode was installed at a 45-degree angle to the thruster shaft, with the cathode orifice around 150 mm above the thruster centerline, and operated at a mass flow rate of 0.29 mg/s. The thruster operated at 1.43 mg/s xenon anode mass flow at 150–250 V. It was operated continuously for over two hours at approximately 400 W without active cooling. A maximum radial magnetic field strength of 0.12 T is achieved along the center line of the anode. Anode potentials of 150–250 V and anode mass flow rates of 0.48–1.43 mg/s resulted in the thrust and anode-specific impulse of 2.4 to 17.4 mN and 500 to 1200 s, respectively. The anode efficiency varied between 12.4% and 25.6% over discharge powers ranging from 47 to 412 W, respectively. The thruster exhibited consistent efficacy across a broad spectrum of operational circumstances. However, at higher voltage of 250 V, instead of the normal diffuse appearance, a bright patch resembling a spike was noticed at the centerline of the thruster. Following a prolonged period of operation, the front wall and anode exhibited the presence of deposited conductive material as well.

The thruster's performance was comparable to that of a traditional HET under identical circumstances, allowing the use of a different design for cube stat operations. The

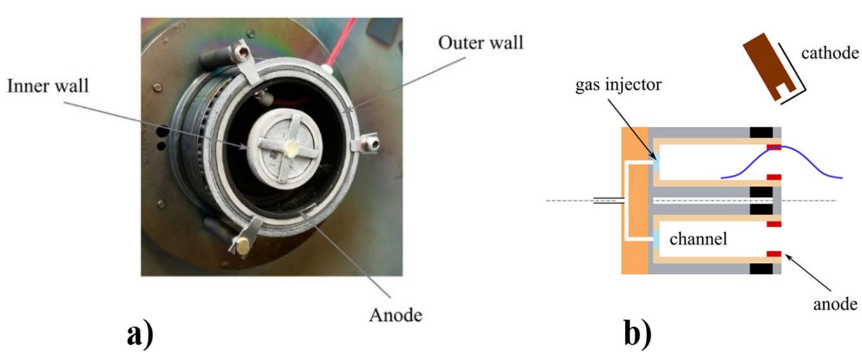

Fig. 13 **a** WL-HET design and **b** Simplified schematic of wall-less thruster concept [23]

authors deemed the thruster to be erosion-free due to the dark anode space and material deposition; nevertheless, further profilometry was necessary to validate this claim.

Narrow Channel HET (NCHT)

A miniaturized HET was developed by Kronhaus [25] at Aerospace Plasma Lab (APL), Techinon, to explore wall-less thruster design for low power conditions. The Narrow Channel HET (NCHT) thruster was developed for use at low voltages and low mass flow rates to aid in studies aimed at better propellant use in very low-power operation modes.

The design of the prototype thruster included a discharge outlet with a mean diameter of 3 cm and a channel width-to-mean diameter ratio of 1:30. The thruster proportions were chosen to retain appropriate gas density at low mass flow rates, resulting in a much narrower and shorter channel than the traditional design. The NCHT used a narrow channel of $h = 1$ mm with a ratio of $h/dmc \approx 1/30$ and assumed a current density of 1000 A/m^2 at the exit instead of standard dimensional scaling that maintains a ratio of channel width to mid-channel diameter of $h/dmc \approx 1/6$ (as observed in SPT-100) [51]. Figure 15 illustrates a schematic representation of the NCHT, which depicts the channel constructed between two concentric metal walls that functioned as the magnetic poles. The channel diameter decreased in size as it approached the exit, resulting in the formation of pointed tips at the poles. This configuration led to the generation of a robust magnetic field and enhanced resistance to erosion of the channel walls. A metal gas distributor served as the anode and the metal walls were held at a negative potential. The cathode was situated 1 cm away from the thruster and had a negative potential of 8 V relative to the ground.

The thruster was operated with a xenon volumetric flow rate of 10 sccm. It underwent testing in low power mode, which employed a maximum discharge voltage of 100 V and a maximum discharge current of 0.45 A. In the experiment, the thruster was operated for a minimum of 30 min. With a maximum power of 15 W and flow rate of 0.38 mg/s, the thruster displayed a thrust level of 1 mN. Increases in mass flow rate resulted in the generation of higher currents while maintaining the same discharge voltage. A discharge current of 0.18 A and discharge voltage of 85 V yielded a specific impulse of 230 s and propellant usage efficiency of 27.6%.

Parametric research verified thruster design theory and found that channel diameter and discharge voltage were the main design parameters. The NCHT operation data suggested that despite the design operating at low power and mass flow rate, it achieved a significant thrust-to-power ratio of 50 μN/W. In comparison to other thrusters that operate at extremely low power, this high thrust-to-power ratio was considered advantageous. As a result, this provides researchers with the incentive to continue their research on the NCHT architecture in order to optimize it for low-power operation.

Comparison between conventional and non-conventional HETs

Non-conventional thruster construction is typically inspired by conventional HETs of similar size or operating power conditions, as shown in Tables 1 and 2. The comparison between the non-conventional HETs and the conventional HETs detailed in the preceding section reveals that, under identical operating power settings, the conventional HETs exhibit greater thrust, as evidenced by the data presented in Fig. 16. At an operational

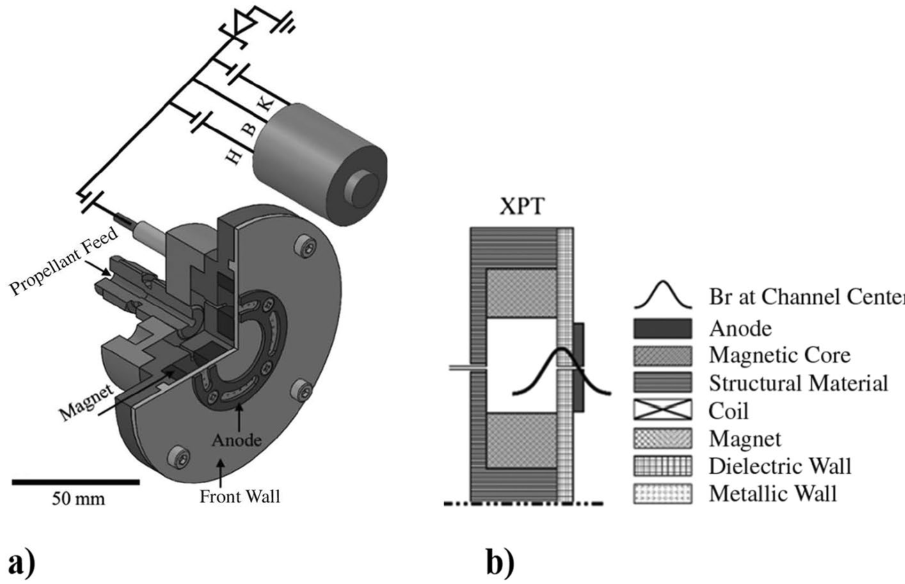

Fig. 14 **a** XPT Cross-sectional View and **b** Schematic cross-sectional view of XPT components [24]

power of 400 W, the XPT wall-less thruster [24] generated a thrust of 15 mN, while the traditional HET KM-32 [52] exhibited a thrust of 18.5 mN under comparable power conditions. An intriguing aspect of this case, as previously discussed, is that the XPT thruster lacks walls due to its wall-less configuration, rendering the effect of channel shape and size on HET performance insignificant. However, it is important to note that the electric and magnetic fields, which govern the dynamics of electrons and ions, are vital for the operation of the thruster. Under the operating scenario when the discharge current ranges are similar, specifically 1.04 A for XPT [24] and 1.26 A for KM-32 [52], it was observed that the discharge voltage for KM-32 [52] was 50% higher compared to XPT [24]. The availability of a higher voltage can lead to improved acceleration capabilities, hence resulting in increased thruster performance and specific impulse, I_{sp}, as depicted in Fig. 17. Although the performance of the non-conventional HET is comparable to or inferior to that of the conventional HET at the same operating power, the latter requires significantly stronger magnetic fields to function. The trend can be attributed to different shapes of the non-conventional channel while maintaining a similar magnetic circuit design; therefore, additional magnetic power is necessary to induce the desired electron motion for accurate ionization. Another comparison was made between non-conventional LHET [16] and conventional BHT-HD-600 [53] operating at same power level of 600 W. The LHET [16] propulsion system demonstrated 2.2 mN thrust with an I_{sp} of 1070 s.

In contrast, the BHT-HD-600 [53] exhibited an exceptionally high thrust of 36 mN, accompanied by an I_{sp} 700 s greater than the LHET [16]. The current closing mechanism distinguishes the thrusters significantly; the LHET is an open drift thruster, while the BHT-HD-600 [53] is a closed drift thruster. The open drift motion of electrons necessitates an exceedingly high magnetic field strength of 1600 G for the LHET [16], in contrast to the typical magnetic field range of 100–800 G. The linear motion pathway and the lack of the mirror effect, both consequences of the radially uniform magnetic field, contribute to a decreased electron collection pathway. Consequently, a stronger magnetic field becomes indispensable to optimize thruster performance and ionization for the desired levels.

Mitigating the influence of thruster size results in using the thrust-to-power ratio, T/P, as the performance metric for HET. Figure 18 shows the relationship between the T/P ratio and efficiency and reveals that the conventional HETs exhibit lower efficiency than non-conventional HETs for comparable T/P ratios. The Racetrack HET BHT-RT-1500 [22] demonstrated an operational efficiency of 41%, whereas the KM-32 [52] and ISCT200-US [65] exhibited 34.9% and 31% efficiencies, respectively. Therefore, the development of BHT-RT-1500 [22] paved the way for further investigation into non-conventional HETs that exhibit promising or comparable functionality. Similarly, with a similar range T/P ratio, the Diverging Cylindrical Thruster achieved 4% more efficiency than standard HET.

In general, while examining the thruster in relation to the mass flow rate of xenon propellant, conventional HET demonstrated a greater T/P ratio Fig. 19. The propellant flow rate of XPT [24] at 1.43 mg/s exhibited a 10% lower T/P compared to KM-32 [52] at 1.40 mg/s. Compared to BHT-200 [48], the Diverging Cylindrical Thruster (DCHT) [21], with a flow rate of 0.894 mg/s, demonstrated an 10% lower T/P ratio. On the other hand, contrary tendencies were also observed, such as the fact that non-conventional HETs had a better T/P ratio. Comparing the SPT-70 [48–51, 54, 55, 57, 61] with the Cylindrical HET [20] at a mass flow rate of 2.5 mg/s, the non-conventional Cylindrical HET [20] exhibited a T/P ratio 20% greater than that of the SPT-70 [57]. However, it is important to note that the T/P ratio should not be regarded as the sole performance indicator. For instance, when comparing the Cylindrical Thruster [20] with the SPT-70 [57], the thrust exhibited by the Cylindrical Thruster was 8 mN.

In contrast, the SPT-70 [57] demonstrated a thrust of 40 mN, which was 400% greater than that of the Cylindrical Thruster [20]. Therefore, when comparing thrusters, it is critical to consider all parameters to identify the most optimized solution as per the mission specifications. A comparison of mass flow rate and efficiency yields mixed results leads to a general conclusion that conventional HETs are more efficient. This performance comparison of non-conventional HET with conventional HET provides insight into the potential for growth in non-conventional HET as well as the potential areas

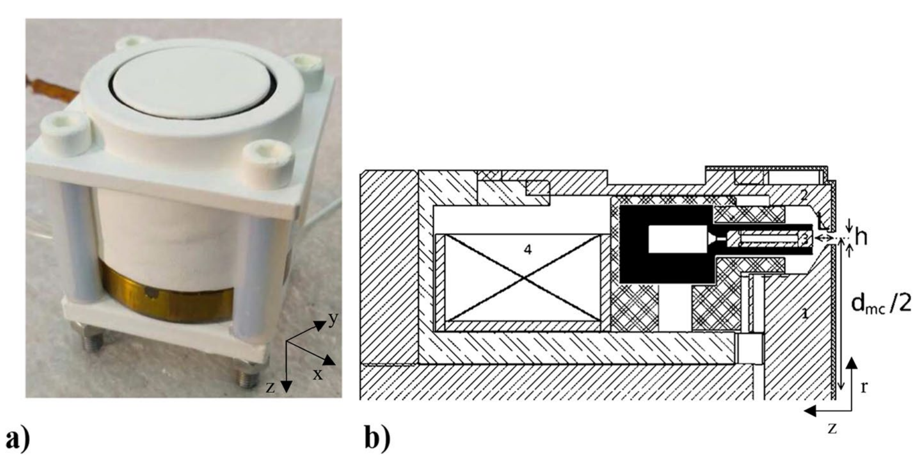

Fig. 15 **a** NCHT and **b** Schematic cross-sectional view of NCHT displaying 1) Inner pole 2) Outer pole 3) Gas distributor 4) Coil [25]

Table 1 Low and mid- power conventional HETs

Thruster	$(m\_a)^{\cdot}$, mg/s	Magnetic Field, G	Power, *W*	Thrust, mN	I_{sp}, s	*T/P*, mN/kW	η, %	References
SPT-50	1.50	180	310	17.3	1280	55.81	35	[54–56]
SPT -70	2.70	200	650	40	1510	61.54	48	[57–59]
SPT-100	5.30	140	1350	83	1600	61.48	50	[57, 60]
TAL D-38	2.36	350–360	766	45.8	1800	59.79	52	[54]
BHT-200	0.83	500	200	12.4	1300	62.00	42	[61]
KM-32	1.40	-	388	18.5	1740	47.68	34.9	[52]
MaSMi-60-(LM1/2)	2.85	-	500	35.8	1440	71.60	24.4	[57, 62]
THT-IV	2.00	200	540	30.5	2300	56.48	40	[63]
BHT-HD-600	2.00	-	600	36	1700	60.00	51	[53]
HEP-300PM	1.38	-	300	16.8	1150	56.00	40.8	[64]
ISCT200-US	1.20	-	360	17	1400	47.22	31	[65]
TCHT-4	0.20	600	66	1.4	1600	21.21	18.1	[66, 67]

- Performance characteristics not available

Table 2 Non-conventional HET performance parameters

Thruster	$(m\_a)^{\cdot}$, mg/s	Magnetic Field, G	Power, *W*	Thrust, mN	I_{sp}, s	*T/P* mN/kW	η, %	References
LHET	0.20	1500	600	2.2	1070	28.76	14.6	[16]
LHET-diamond	0.60	800	260	-	-	-	-	[17]
LGIT	1.47	500	1170	20	1400	17.09	12	[18]
PHT	0.25	500	500	-	-	-	-	[19]
CHT	2.50	600–1400	100	8	-	80.00	22	[20]
DCHT	0.83	3000–5000	250	13.4	1641	53.60	44.5	[21]
BHT-RT-1500	12.00	-	1675	84	1678	50.15	41	[22]
WL-HET	1.00	-	-	-	-	-	-	[23]
XPT	1.43	1000	400	15	1200	37.50	25	[24]
NCHT	0.10	-	40	1		25.00	-	[25]

- Performance characteristics not available

where non-conventional HET falls short. In order to address the growth area of non-conventional HETs, it is crucial to investigate the problematic issues or components that comprise non-conventional HET.

Challenges in non-conventional channel shape

The analysis of non-conventional HETs yielded valuable findings regarding the favorable performance of the HETs. However, it is crucial to emphasize the areas that require development in order to forward the research of these alternative HET channel designs. In this section, the issues observed in the non-conventional HET performance investigations and the likely causes based on our working knowledge of plasma physics have been discussed. The primary challenges encountered by these unconventional designs were primarily related to 1) stability. 2) beam divergence, and 3) wall erosion.

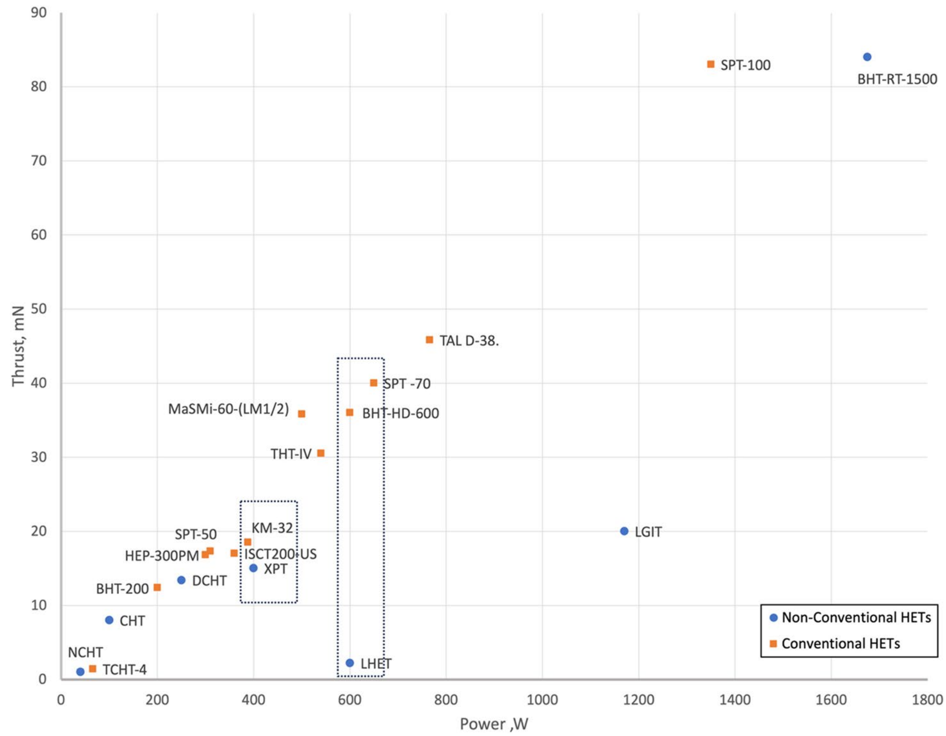

Fig. 16 Conventional and non-conventional HET thrust as a function of discharge power

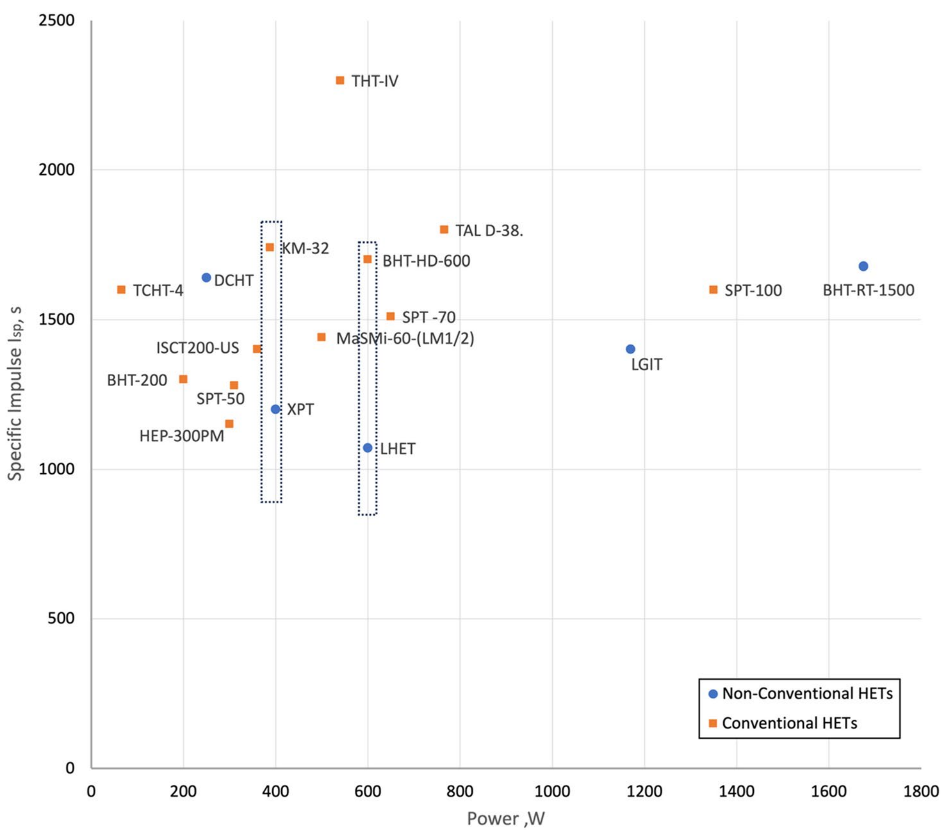

Fig. 17 Conventional and non-conventional HET I_{sp} as a function of discharge power

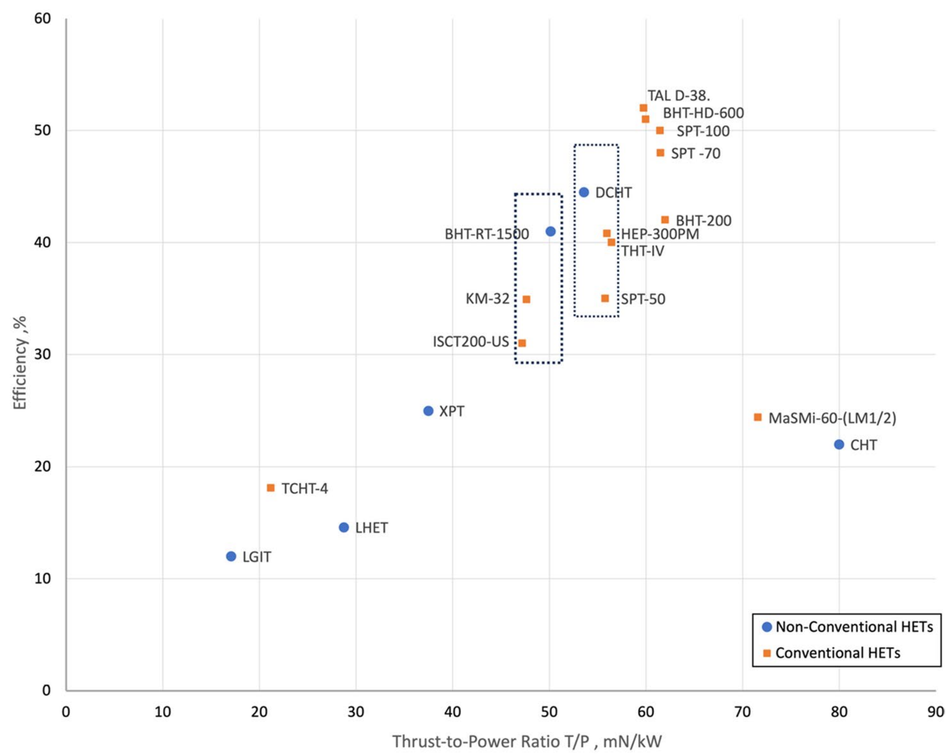

Fig. 18 Conventional and Non-conventional HET η as a function of thrust-to-power ratio

Stability

Stable functioning was one of the critical problems discovered while researching non-traditional HET designs. Stability is one of the most important requirements for the HET, as stable continuous operation is necessary for sustaining plasma during thruster operation. When considering non-conventional design thrusters, the linear HET faces the most significant challenges when maintaining a sustained plasma discharge. When considering the LHET [16], the presence of pulsed plasma during thruster operation posed a challenge in maintaining a discharge and achieving sustained operating conditions. However, the study failed to give sufficient data explaining the pulsed behavior. Comparable circumstances were noted in the functioning of LGIT [18]. The study's findings indicated that an electric short between the anode and screen led to the thruster operating erratically, with a brief period of stability lasting no longer than three minutes. The cause of unstable behavior can be a result of charge accumulation encountered due to the current closing in the linear thruster configuration. The closure of the circuit is contingent upon the electron drift mechanism within the channel as electrons traverse the magnetic field lines. An in-depth examination of a linear design to comprehend electron dynamics in the channel may provide additional insight into the instability observed in non-conventional linear HETs. Aside from linear designs, the inclusion of circular parts in the channel or the absence of a channel entirely also plays a role in ensuring the stable functioning of the thruster. Despite being closed drift, the racetrack thruster design demonstrated a variety of instabilities that differed from those reported in traditional HET. Several instabilities identified were associated with operational modes, including breathing mode and quasi-spoke mode [49]. The inconsistency in the output of the breathing mode intensity oscillations is attributed to the geometric characteristics of the pseudo-linear (racetrack) thruster, in contrast to the cylindrical design. In conventional cylindrical HET configurations, the Hall current is capable of traversing the channel at a consistent velocity; however, this did not hold true for non-conventional racetrack designs. This phenomenon can be attributed to the compression of magnetic field lines in the curved sections, as opposed to the straight sections. The pseudo linear hall thruster demonstrated the capability to generate spokes in specific sections of the channel, specifically a quasi-spoke mode, in which the spoke would travel at different speeds around the channel. Therefore, pseudo linear(racetrack) Hall thruster exhibited a dissimilar ionization rate between the circular and straight sections of the channel, which is not typical of conventional HETs. This highlights the influence of the magnetic field variation on the performance of the HET.

Beam divergence

Beam divergence of plasma associated with a HET exhaust is dependent on the thruster channel, magnetic field topology, and charge particle energy distribution among other aspects of HET operation. All these parameters influence the acceleration and ionization processes that generate the plasma plume and, consequently, the efficacy of the HET. The beam divergence of the plume indicates the number of focused ions departing from the thruster to generate the intended propulsion. Lower beam divergence offered a focused flow of electrons, resulting in greater divergence efficiency for the thruster and improved thrust and I_{sp} performance. The operation of the thruster can be significantly affected by beam divergence, particularly in terms of the charge deposition on the spacecraft and the overall impact on thruster performance [17]. When attempting to utilize multiple HETs for propulsion, increased beam divergence may give rise to packaging challenges as a result of the interaction between the thruster plasma emissions. The investigation of non-conventional HETs revealed that most non-conventional HETs had larger beam divergence than conventional HETs. The rectangular geometry of the linear thruster design caused beam divergence to vary around different parts of the channel thruster, with an estimated divergence of 15° in the transverse (parallel to B) direction and 60° in the lateral (parallel to $E \times B$) direction. The standard convention HET has a beam divergence of approximately 30° or less, resulting in a significant rise in beam divergence. There was, however, insufficient relevant evidence to confirm the precise cause of the observed effects. Following an examination of non-conventional HET configurations, including racetrack and linear, the magnetic field topology associated with these configurations is believed to be a fundamental design element contributing to the increased beam divergence. Variations in the curvature and magnitude of the magnetic field can produce a radial electric field component, which is responsible for potential plume divergence [68]. The formation of the radial electric field results from the magnetic mirror force's incapacity to impede the electron's motion toward the wall. As a result, electrons tend to collide with the channel's outer wall, accumulating potential gradients that create the radial electric field.

Consequently, the radial electric field attracts ions to the wall, leading to the occurrence of higher beam divergence. The magnetic field topology connected with the linear and racetrack thrusters is constructed using a magnetic circuit pattern applied to conventional HET, which does not provide the best configuration. The research conducted by WL-HET

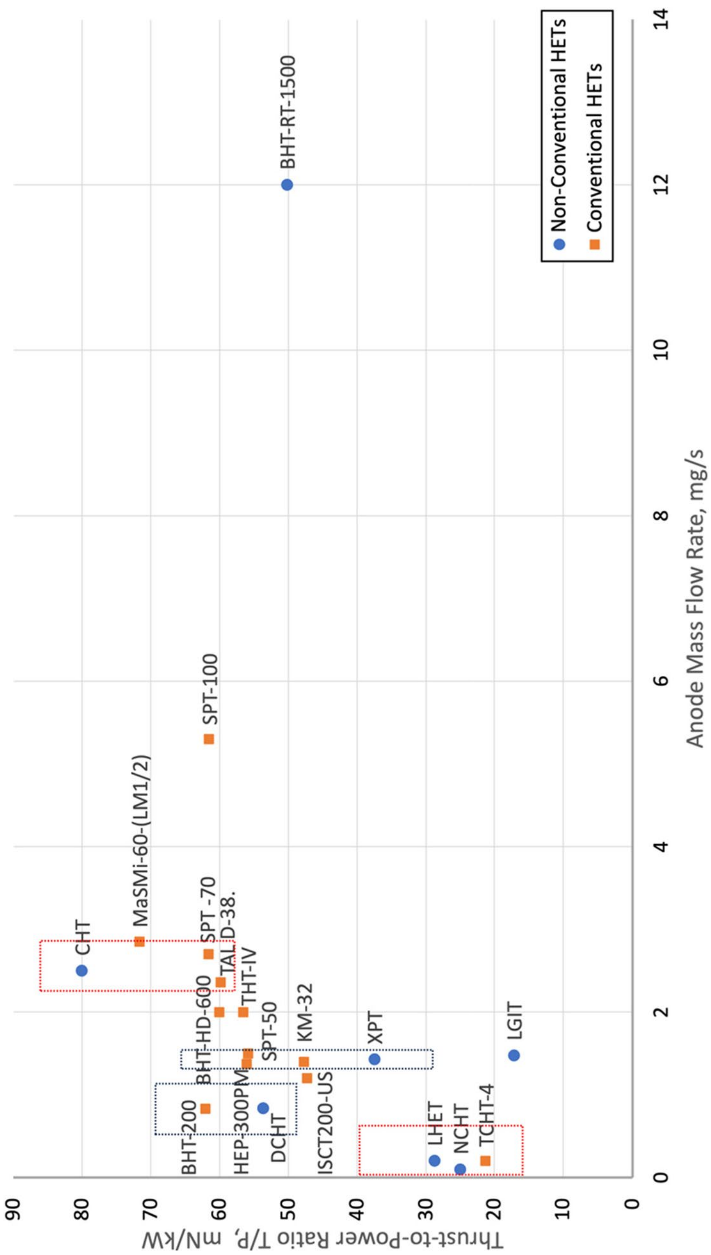

Fig. 19 Conventional and non-conventional HET thrust-to-power ratio T/P variation with ***(m_a)***

[23] also proposed that the divergence seen might be an attribute to the magnetic field and that adjusting the magnetic field could optimize thruster performance.

Erosion: wall losses

Section II, an overview of the various non-conventional HETs, addresses potential issues about the thruster's long-term operation due to erosion effects. While the majority of thrusters were not tested for an extended time to observe the effects due to stability issues, a racetrack channel configuration study [49] offers valuable insights into erosion processes. The channel erosion is visible in the darkening of the discharge channel wall, as shown in Fig. 20, and is primarily assessed based on the magnitude of power deposition on the channel's wall. Although visual inspections have identified areas of power or electron bombardment on the channel walls through erosion of the channel insulator at the observed hot spots, the underlying cause of these wall losses remains uninvestigated. Wall losses are the dissipation of incoming particles' kinetic energy as they collide with the wall. The evaluation of wall losses considers the high energy of electrons and ions.

Numerous studies assess energy deposition on the channel wall due to sputtering as a function of the sheath potential, electron temperature, and radial ion velocity. Jianfei [69] estimates the energy loss in the discharge channels by utilizing sheath potential and electron temperature to assess the efficacy of HETs.

$$P_a = \sum_{j=1}^{n_{ew}} \left(q_{e,kinetic} + \frac{3kT_e}{2} - e\phi \right)_j + \sum_{j=1}^{n_{iw}} \left(q_{i,kinetic} + \frac{3kT_i}{2} - e\phi \right)_j \tag{2}$$

$E \times B$ drift and inertial effects of electron motion during the transition from a straight section with a uniform magnetic field to a curved section with a radially varying magnetic field account for the increased power deposition. Although the visual inspection revealed minimal erosion, the continual damage will have a detrimental impact on the thruster's lifespan. The existence of unstable operation and hot spots can lead to increased degradation of the thruster, resulting in a shorter lifespan compared to conventional HETs.

Future research prospective

Examination of non-conventional magnetic fields and their efficacy compared to conventional HETs sheds light on the domains that require further investigation during the development of non-circular channels. Through the various studies reviewed it is established that understanding the particle dynamics in the channel for various channel shapes and optimizing the magnetic field topology can aid in advancing the development of such thrusters for stacking or low-power conditions.

The review of linear HETs reveals that it is possible to achieve equivalent or comparable performance to traditional HETs. As observed in the closed drift motion process of electrons in conventional HETs, the electrons must traverse toward the anode in order to close the electron Hall current circuit. In the case of open drift thrusters Linear HET, the electrons experience anomalous axial mobility due to either plasma fluctuations or collisions with channel walls. The magnetic field is a significant factor in plasma fluctuations and can impact the stable operation of HET. The conventional HETs, being closed drift thrusters, allow efficient ionization, resulting in better propellant utilization. However, the linear, racetrack, and wall-less thrusters show that electron motion is open drift, not spatially constrained, and has azimuthal changes, making HET operation challenging. The open drift thrusters were unable to provide extended transportation duration for electrons within the channel, hence impacting the efficiency of ionization. The confinement of electrons in a geometrical space is crucial for achieving efficient ionization and acceleration of charged particles. The wall-less thruster failed to achieve the desired performance outcomes due to inefficient acceleration. The observed azimuthal differences in racetrack HET are caused by the unique shape of the channel, which leads to non-uniform electron mobility. This, in turn, results in changes in the plasma plume across the channel. The non-uniformity in the electron dynamics across the channel must be explored while developing non-conventional HET.

Through the review of the racetrack HET, the essential role that the magnetic field played in the operation of HET is highlighted. The racetrack HET exhibits non-uniform dispersion of magnetic field lines along its channel during operation. Compacted magnetic field lines result in an increase in the magnetic flux density in circular sections contribute to an increase in the intensity of the magnetic field within the section. Changes in the magnetic field tend to impact the inertial motion of electrons emanating from the linear section of the racetrack channel. The electrons coming from the straight section encounter a drastic change in the strength and direction of the magnetic field, which forces the electron to deviate from the straight path motion. However, because of the high velocity of the electron and the abrupt change in its trajectory within the channel, the inertial velocity of electron being high delays the reaction of the electron to the curved geometry of the channel. Consequently, the electron deviates from the theoretically expected direction of motion. The alteration in motion leads to the accumulation of charge at the beginning of each circular segment, hence increasing the number density, frequency of collisions, and temperature. The rise in temperature leads to an escalation in the thermal erosion of these wall sections, a phenomenon that is considered unfavorable. To allow better operation of non-conventional HETs the magnetic field topology requires modification and optimization with respect to the channel shape. Studying the geometry of the channel and the magnetic circuit governing electron transport in the channel is thus crucial for the advancement of non-convention HET channel design.

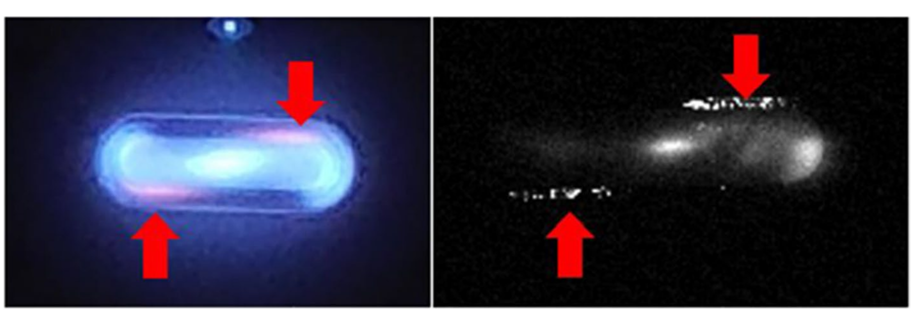

Fig. 20 The non-uniform erosion observed in the pseudo linear thruster, as reported in reference [49]

Conclusion

This review analysis offers insights into the diverse range of non-conventional HETs, each featuring different channel cross-section geometries including linear, racetrack, and wall-less configurations. This study focuses on the performance evaluation of non-traditional thrusters and presents a comparative analysis with conventional hall thrusters operating in low to mid-power configurations. Although several of the discussed research efforts failed to reach their goals due to limited funding, the review offers crucial insights into the potential impact of non-uniform magnetic fields on HET performance via investigations into non-conventional channel shapes. The non-conventional HET's performance, comparable to that of conventional thrusters, offers a viable avenue for investigating the feasibility of employing it in subsequent flights. In order to gain a deeper comprehension of the thruster, this discussion addresses the drawbacks observed in non-conventional thrusters, specifically focusing on stability and erosion concerns inherent in these designs. The study compels us to optimize the magnetic field circuit according to each channel shape and comprehend the dynamics of electrons for enhanced performance. With design optimization, increased use of HET for low orbit maneuvering and development of non-conventional HET operating in low-mid power configuration can provide a better-stacking alternative in the future.

Nomenclature

I_{d} discharge current, A
V_{d} discharge Voltage, V
I_{sp} Specific impulse, s
(m_a) anode mass flow rate, mg/s.
η thruster efficiency, %
h height of thruster channel, mm.
w width of thruster channel, mm.
d diameter of thruster channel, mm.
l length of channel, mm.
ϕ sheath potential, V
P_a energy loss to the wall, J
n_{ew} number of electrons incident to the wall.
n_{iw} number of ions incident to the wall.
T_i ion temperature, K
$q_{(e,kinetic)}$ kinetic energy of electrons,J
$q_{(i,kinetic)}$ kinetic energy of ions, J
r_L Larmor radius, mm.
B magnitude of magnetic field, G
m mass of charged particle, kg.
$v\_\perp$ velocity of charges particle perpendicular to magnetic field, m/s.
q charge of particle, C

Appendix

Table 3 Conventional HET characteristics

Thruster	Propellant	Channel Dimensions	I_d, A	V_d, V	Magnetic field, mT	References
SPT-50	xenon	d = 5 cm, w = 10 mm	1.5	280	15	[52, 53]
SPT-70	xenon	d = 7 cm, w = 17 mm	2.17	300	-	[54, 65]
SPT-100	xenon	d = 100 cm, w = 15.5 mm	4.5	300	-	[54]
TAL D-38	xenon	d = 38 mm	2.52	300	35–36	[52]
BHT-200	xenon	d = 21 mm, w = 8 mm	0.8	250	50	[55]
KM-32	xenon	d = 32 mm, w = 6 mm	0.38–1.26	200–400	-	[56]
MaSMi-60-(LM1/2)	xenon	d = 6 cm	1.67	300	-	[54, 57]
THT-IV	xenon	d = 70 mm, w = 14, h = 15—30 mm	2.7	200	-	[58]
BHT-HD-600	xenon	d = 150 mm, w = 120 mm, h = 120 mm	2	300	-	[59]
HEP-300PM	xenon	-	1.36	220	-	[60]
ISCT200-US	xenon	-	1.2	300	-	[61]
TCHT-4	xenon	r = h = 7 mm	0.188	350	-	[62]

- Data unavailable, l = length, w = width, h = height, r = radius, d = diameter

Table 4 Non-conventional HET characteristics

Thruster	Propellant	Channel Dimensions	I_d, A	V_d, V	Magnetic field, G	References
LHET	xenon	w = 3 mm	0.51	150	1600	[16]
LHET-diamond	xenon	l = 50.8 mm, w = 3.2 mm, h = 12.7 mm	1.03	250	800	[17]
LGIT	xenon	l = 198 mm, w = 16 mm, h = 22 mm	3.9	300	500	[18]
PHT	xenon	l = 203 mm, w = 25 mm, h = 108 mm	5	100	500	[19]
CHT	xenon	r = 9 cm, w = 2.5 cm	0.5–1	250	600–1400	[20]
DCHT	xenon	d = 88 mm (max)	0.5–1	250–550	5000	[21]
BHT-RT-1500	xenon	-	4.8	350	-	[22]
WL-HET	xenon	-	0.45	100	-	[23]
XPT	xenon	-	1.05	200	-	[24]
NCHT	xenon	$w = 1$ mm, $d = 30$ mm	2	150–200	1000	[25]

Authors' contributions
Conceptualization: Chhavi Chhavi and Mitchell L.R. Walker; literature search and data analysis: Chhavi Chhavi; Writing—original draft preparation: Chhavi Chhavi; Writing -review and editing: Chhavi Chhavi and Mitchell L.R. Walker. The author(s) read and approved the final manuscript.

Funding
No Funding was used for this research.

Availability of data and materials
No datasets were generated or analysed during the current study.

Declarations

Competing interests
"Mitchell Walker is an Editorial Board member of Journal of Electric Propulsion, and they were not involved in the journal's review of, or decisions related to, this manuscript."

Received: 24 February 2024 Accepted: 3 June 2024
Published online: 18 June 2024

References

1. Koppel CR, Estublier D (2005) The SMART-1 Hall effect thruster around the moon: in flight experience. Presented at the 29th International Electric Propulsion Conference, IEPC Paper 2005–119. Electric Rocket Propulsion Society, Princeton
2. Hofer R (2010) High-specific impulse operation of the BPT-4000 Hall thruster for NASA science missions. 46th AIAA/ASME/SAE/ASEE Joint Propulsion Conference & Exhibit. p 6623
3. Hall SJ (2018) Characterization of a 100-kw class nested-channel Hall thruster. Ph.D. Dissertation, University of Michigan, Ann Arbor
4. Piragino A, Leporini A, Giannetti V, Pedrini D, Rossodivita A, Andreussi T, Andrenucci M (2017) Characterization of a 20 kW-class Hall effect thruster. 35th International Electric Propulsion Conference, IEPC-2017–381. Electric Rocket Propulsion Society, Atlanta
5. Morozov AI, Savelyev VV (2000) Fundamentals of stationary plasma thruster theory. Reviews of plasma physics. Springer, Boston, pp 203–391
6. Saleh J, Geng F, Ku M, Walker M (2017) Electric propulsion reliability: statistical analysis of on-orbit anomalies and comparative analysis of electric versus chemical propulsion failure rates. Acta Astronaut 139:141–156. https://doi.org/10.1016/j.actaastro.2017.06.034. ISSN 0094-5765
7. Lev D, Myers R, Lemmer K, Kolbeck J, Koizumi H, Polzin K (2019) The technological and commercial expansion of electric propulsion. Acta Astronaut 159:213–227. https://doi.org/10.1016/j.actaastro.2019.03.058. ISSN 0094-5765
8. Levchenko I, Goebel D, Bazaka K (2022) Electric propulsion of spacecraft. Phys Today 75(9):38–44. https://doi.org/10.1063/PT.3.5081
9. Curzi G, Modenini D, Tortora P (2020) Large constellations of small satellites: a survey of near future challenges and missions. Aerospace 7(9):133. https://doi.org/10.3390/aerospace7090133
10. Potrivitu G, Yufei R, Muhammad C, Oleksii X, Luxiang H, Shiyong XuS (2020) A review of low-power electric propulsion research at the space propulsion centre Singapore. Aerospace 7(6):67. https://doi.org/10.3390/aerospace7060067
11. Cusson SE, Georgin MP, Dragnea HC, Dale ET, Dhaliwal V, Boyd ID, Gallimore AD (2018) On channel interactions in nested Hall thrusters. J Appl Phys 123(13):133303. https://doi.org/10.1063/1.5028271
12. Duchemin O, Lorand A, Notarianni M, Valentian D, Chesta E (2007) Multi-channel hall-effect thrusters: mission applications and architecture trade-offs. 30th International Electric Propulsion Conference (IEPC), IEPC-2007–227. Florence
13. Peterson PY (2004) The development and characterization of a two-stage hybrid Hall/ion thruster. Ph.D. Dissertation, University of Michigan
14. Hofer RR et al (2001) A high specific impulse two-stage Hall thruster with plasma lens focusing. The 27th International Electric Propulsion Conference, IEPC-01–036 Pasadena, CA
15. Dubois L, Gaboriau F, Liard L, Harribey D, Hénaux C, Garrigues L, Hagelaar GJH, Mazouffre S, Boniface C, Boeuf JP (2008) D-HALL, a new double stage Hall thruster design. I. Principle and hybrid model of ID-HALL. Phys Plasmas 25(9)
16. Hargus W Jr, Cappelli M (1998) Development of a linear Hall thruster. 34th AIAA/ASME/SAE/ASEE Joint Propulsion Conference and Exhibit. ARC, Cleveland
17. Meezan N et al (2001) Linear geometry hall thruster with boron nitride and diamond walls. The 27th International Electric Propulsion Conference, Pasadena, CA, 15–19 October
18. Beal B, Gallimore AG (2001) Development of the linear gridless ion thruster. 37th AIAA/ASME/SAE/ASEE Joint Propulsion Conference and Exhibit. ARC, Salt Lake City
19. Rovey JL et al (2007) A planar Hall thruster for investigating electron mobility in ExB devices. Proceedings of the 30th International Electric Propulsion Conference Proceedings (2007, Florence, Italy). Electric Rocket Propulsion Society
20. Raitses Y, Smirnov A, Fisch N (2006) Cylindrical Hall Thrusters. 37th AIAA Plasmadynamics and Lasers Conference. San Francisco. https://doi.org/10.2514/6.2006-3245
21. Courtney DG, Martínez-Sánchez M (2007) Diverging Cusped-Field Hall Thruster (DCHT). Proceedings of the 33rd International Electric Propulsion Conference (IEPC-2007). Electric Rocket Propulsion Society, Florence
22. Pote B, Hruby V, Tedrake R (2000) Performance of a multi-kilowatt non-circular discharge Hall thruster. 36th AIAA/ASME/SAE/ASEE Joint Propulsion Conference and Exhibit. Las Vegas. https://doi.org/10.2514/6.2000-3249
23. Mazouffre S, Tsikata S, Vaudolon J (2014) Development and experimental characterization of a wall-less Hall thruster. J Appl Phys 116(24):243302
24. Karadag B, Cho S, Funaki I, Hamada Y, Komurasaki K (2018) External discharge plasma thruster. J Propul Power 34(4):1094–1096
25. Kronhaus I, Linossier A (2018) Experimental characterization of the narrow channel Hall thruster. Plasma Sources Sci Technol 27:124005https://doi.org/10.1088/1361-6595/aaec65
26. Dunaevsky A, Raitses Y, Fisch NJ (2003) Secondary electron emission from dielectric materials of a Hall thruster with segmented electrodes. Phys Plasmas 10:2574
27. Choueiri EY (2001) Fundamental difference between the two Hall thruster variants. Phys Plasmas 8:5025–5034
28. Dunaevsky A, Raitses Y, Fisch NJ (2003) Yield of secondary electron emission from ceramic materials of Hall thruster with segmented electrodes. In Proceedings of the 28th International Electric Propulsion Conference. Electric Rocket Propulsion Society, Toulouse, p 1–7
29. Brown NP, Walker MLR (2020) Review of plasma-induced Hall thruster erosion. Appl Sci 10(11):3775. https://doi.org/10.3390/app10113775

30. Jacobson DT, Manzella DH, Hofer RR, Peterson PY (2004) NASA's 2004 Hall thruster program. 40th AIAA/ASME/SAE/ASEE Joint Propulsion Conference & Exhibit, Fort Lauderdale. https://doi.org/10.2514/6.2004-3600. AIAA Paper 2004-3600
31. Brown DL (2009) Investigation of low discharge voltage Hall thruster characteristics and evaluation of loss mechanisms. Ph.D. Dissertation, Dept. of Aerospace Engineering, Univ. of Michigan, Ann Arbor
32. Pérez Grande D (2018) Fluid modeling and simulation of the electron population in Hall effect thrusters with complex magnetic topologies. Ph.D, Dpto. de Bioingenería e Ingeniería Aeroespacial Escuela Politécnica Superior
33. Khayms V, Martinez-Sanchez M (2000) Fifty-watt Hall thruster for microsatellites. Micropropulsion Small Spacecraft 187:233–254 Progress in Astronautics and Aeronautics. AIAA, Reston, VA
34. Smirnov A, Raitses Y, Fisch N (2003) Enhanced ionization in the cylindrical Hall thruster. J Appl Phys 94(2):852–857. https://doi.org/10.1063/1.1585114
35. Smirnov A, Raitses Y, Fisch NJ (2004) Electron cross-field transport in a low-power cylindrical Hall thruster. Phys Plasmas 11(11):4922–4933. https://doi.org/10.1063/1.1791639
36. Shirasaki A, Tahara J, Yoshikawa T (2003) Operational characteristics of cylindrical Hall thrusters. The 28th International Electric Propulsion Conference. Toulouse. EPC paper 2003–51. ibid. "Plume measurements and miniaturization of Hall thrusters with circular cross-sectional discharge chambers," IEPC paper 2005–051, the 29th International Electric Propulsion Conference, Electric Rocket Propulsion Society, Princeton, NJ, Oct. 2005
37. Koch N, Harmann HP, Kornfeld G (2005) Development and test status of the THALES high efficiency multistage plasma (HEMP) thruster family. Proceedings of the 29th International Electric Propulsion Conference. Electric Rocket Propulsion Society, Princeton, IEPC Paper 2005–297
38. Kim H, Lim Y, Choe W, Seon J (2014) Effect of multiply charged ions on the performance and beam characteristics in annular and cylindrical type Hall thruster plasmas. Appl Phys Lett 105(14):144104. https://doi.org/10.1063/1.4897948
39. Raitses Y, Fisch N (2001) Parametric investigations of a nonconventional Hall thruster. Phys Plasmas 8(5):2579–2586. https://doi.org/10.1063/1.1355318
40. Smirnov A, Raitses Y, Fisch N (2005) The effect of magnetic field on the performance of low-power cylindrical Hall thrusters. The 28th International Electric Propulsion Conference. Electric Rocket Propulsion Society, Princeton, IEPC paper 2005–099. ibid "Electron Cross-Field Transport in a 100 W Cylindrical Hall Thruster", IEPC-2005–098
41. Hruby V, Monheiser J, Pote B, Freeman C, Connolly W (1999) Low power, Hall thruster propulsion system. 26th International Electric Propulsion Conference. Electric Rocket Propulsion Society, Kitakyushu IEPC-99–092
42. Jacobson D, Jankovsky R (1998) Test results of a 200W class Hall thruster. 34th AIAA/ASME/SAE/ASEE Joint Propulsion Conference and Exhibit. ARC, Cleveland. https://doi.org/10.2514/6.1998-3792. AIAA 1998–3792
43. Belikov M, Gorshkov O, Muravlev V, Rizakhanov R, Shagayda A, Shnirev A (2001) High performance low power Hall thruster. 37th AIAA/ASME/SAE/ASEE Joint Propulsion Conference and Exhibit, AIAA-2001-3780, ARC, Salt Lake City. https://doi.org/10.2514/6.2001-3780
44. Bugrova A, Desiatskov A, Kaufman H, Kharchevnikov V, Morozov A, Zhurin V (2001) Design and Experimental Investigation of a Small Closed Drift Thruster. 27th International Electric Propulsion Conference. Electric Rocket Propulsion Society, Pasadena, IEPC paper 01–344–2
45. Bugrova A, Desiatskov A, Kaufman H, Kharchevnikov V, Morozov A, Zhurin V (2003) An improved small closed drift thruster with both conduction and dielectric RIC channels. Proceedings of the 28th International Electric Propulsion Conference. Toulouse. IEPC paper 03–0263
46. Kornfeld G, Koch N, Harmann H (2004) New performance and reliability results of the Thales HEMP thruster. 4th International Spacecraft Propulsion Conference. Electric Rocket Propulsion Society, Cagliari
47. Koch N, Harmann HP, Kornfeld G (2005) Development and test status of the THALES High Efficiency Multi-stage Plasma (HEMP) thruster family. 29th International Electric Propulsion Conference. Princeton University
48. Beal B, Gallimore A, Haas J, Hargus W (2004) Plasma properties in the plume of a Hall thruster cluster. J Propul Power 20(6):985–991. https://doi.org/10.2514/1.3765
49. Sheets BA (2018) Pseudo linear Hall effect thruster characterization through potential, magnetic, and optical measurements. Ph.D. Dissertations, Department of Aeronautics and Astronautics, Air Force Institute of Technology. 1784
50. Vaudolon J, Mazouffre S, Hénaux C, Harribey D, Rossi A (2015) Optimization of a wall-less Hall thruster. Appl Phys Lett 107:174103. https://doi.org/10.1063/1.4932196
51. Kim V et al (2001) Electric propulsion activity in Russia. 27th International Electric Propulsion Conference. Electric Rocket Propulsion Society, Pasadena, IEPC-01–05
52. Belikov MB, Gorshkov OA, Dyshlyuk EN, Lovtzov AS, Shagayda AA (2007) Development of low-power Hall thruster with a lifetime up to 3000 hours. 30th Int. Electric Propulsion Conf. Florence. p 2007–129
53. Hruby V, Monheiser J, Pote B, Rostler P, Kolencik J, Freeman C (1999) Development of low power Hall thrusters. 30th Plasmadynamic and Lasers Conference. Norfolk. https://doi.org/10.2514/6.1999-3534. AIAA 1999–3534
54. Manzella D, Oleson S, Sankovic J, Haag T, Semenkin A, Kim V (1996) Evaluation of low power Hall thruster propulsion. 32nd Joint Propulsion Conference and Exhibit. Lake Buena Vista. https://doi.org/10.2514/6.1996-2736. AIAA 1996–2736
55. Saevets P, Semenenko D, Albertoni R, Scremin G (2017) Development of a long-life low-power Hall thruster. 35th International Electric Propulsion Conference. Georgia Institute of Technology, Atlanta Paper No. IEPC-2017–38
56. Guerrini G, Micaunt C, Dubek M, Vesselovzorov AN, Bacal M (1997) Characterization of plasma inside the SPT-50 channel by electrostatic probes. Presented at the 25th International Electric Propulsion Conference. Electric Rocket Propulsion Society, Cleveland
57. Conversano RW, Goebel DM, Hofer RR, Arora N (2017) Performance enhancement of a long-life, low-power hall thruster for deep-space smallsats. 2017 IEEE Aerospace Conference. Big Sky. p 1-12. https://doi.org/10.1109/AERO.2017.7943577
58. Clauss C, Tilley D, Barnhart D (1995) Benefits of low-power stationary plasma thruster propulsion for small satellites. Technical Report. Air Force Research Laboratory (AFMC). Digital Commons-Elsevier, Berkeley
59. Sullivan R (2010) The physics of high-velocity ions in the Hall thruster near-field. Ph.D. Dissertation, CaliforniaInstitute of Technology, Pasedena

60. Koo J, Boyd I. Computational model of an SPT-100 thruster. Presented at the 28th International Electric Propulsion Conference. Toulouse
61. Beal BE, Gallimore AD, Hargus WA (2005) Plasma properties downstream of a low-power Hall thruster. Phys Plasmas 12(12):123503. https://doi.org/10.1063/1.2145097
62. Conversano RW (2015) Low-power magnetically shielded Hall thrusters. Ph.D. Dissertation, University of California, Los Angeles
63. Tahara H, Fujioka T, Shirasaki A, Yoshikawa T (2003) Simple one-dimensional calculation of Hall thruster flowfields. 28th International Electric Propulsion Conference. Electric Rocket Propulsion Society, Toulouse, IEPC 03–016
64. Ma D, Ding Y, Wang L, Xu F, Li H, Wei L, Yu D (2022) Experimental study on the influence of magnetic inclination in plume region on performance of low-power Hall thruster. Vacuum 195:110673. https://doi.org/10.1016/j.vacuum.2021.110673
65. Grimaud L, Mazouffre S (2018) Performance comparison between standard and magnetically shielded 200 W Hall thrusters with BN-SiO2 and graphite channel walls. Vacuum 155:514–523. https://doi.org/10.1016/j.vacuum.2018.06.056
66. Tahara H, Tonari T (2009) Performance characteristics of very low power cylindrical hall thrusters. 31st International Electric Propulsion Conference. University of Michigan, Electric Rocket Propulsion Society, Michigan, IEPC-2009–272
67. Ikeda T, Togawa K, Nishida T, Tahara H (2011) Research and development of very low power cylindrical Hall thrusters for nano-satellites. Presented at the 32nd International Electric Propulsion Conference. Wiesbaden
68. Baranov VI et al (1997) Energy balance and role of walls in ACDE. 25thInternational Electric Propulsion Conference. Electric Rocket Propulsion Society, Cleveland, IEPC 97–060
69. Long J, Zhang T, Sun M, Liu M (2017) Numerical study on energy loss in discharge channel of Hall thruster. International Electric Propulsion Conference. Electric Rocket Propulsion Society, Atlanta

Publisher's Note